AD_____

Award Number:

W81XWH-09-1-0742

TITLE:

Safe Gene Therapy for Type 1 Diabetes

PRINCIPAL INVESTIGATOR:

Massimo Trucco, M.D.

CONTRACTING ORGANIZATION:

University of Pittsburgh
Pittsburgh, PA 15213

REPORT DATE:

October 2010

TYPE OF REPORT:

Annual

PREPARED FOR: U.S. Army Medical Research and Materiel Command
               Fort Detrick, Maryland 21702-5012

DISTRIBUTION STATEMENT:

     X Approved for public release; distribution unlimited

REPORT DOCUMENTATION PAGE

1. REPORT DATE (DD-MM-YYYY) 01-10-2010	2. REPORT TYPE Annual	3. DATES COVERED (From - To) 28 September 2009 —27 September 2010

4. TITLE AND SUBTITLE
Safe Gene Therapy for Type 1 Diabetes

5a. CONTRACT NUMBER

5b. GRANT NUMBER
W81XWH-09-1-0742

5c. PROGRAM ELEMENT NUMBER

6. AUTHOR(S)

Massimo Trucco, M.D.

5d. PROJECT NUMBER

5e. TASK NUMBER

5f. WORK UNIT NUMBER

7. PERFORMING ORGANIZATION NAME(S) AND ADDRESS(ES)

University of Pittsburgh, The

Pittsburgh, PA 15213-3320

8. PERFORMING ORGANIZATION REPORT NUMBER

9. SPONSORING / MONITORING AGENCY NAME(S) AND ADDRESS(ES)
U.S. Army Medical Research
and Materiel Command
Fort Detrick, MD 21702-5012

10. SPONSOR/MONITOR'S ACRONYM(S)

11. SPONSOR/MONITOR'S REPORT NUMBER(S)

12. DISTRIBUTION / AVAILABILITY STATEMENT
Approved for public release; distribution unlimited.

13. SUPPLEMENTARY NOTES

14. ABSTRACT   In light of accumulating evidence that the endocrine pancreas has regenerative properties, that hematopoietic chimerism can abrogate destruction of beta cells in autoimmune diabetes, and that in this way physiologically-sufficient endogenous insulin production can be restored in clinically-diabetic NOD mice, recapitulating what has also been sporadically seen in humans, we originally proposed to test reliable and clinically translatable alternatives able to re-establish euglycemia in diabetic patients. Instead of relying on the risky allogeneic BM transplantation to obliterate the autoimmune process that causes type 1 diabetes, we originally proposed to reconstitute, by gene supplantation, susceptible (non-Asp57+) NOD mice with their own BM genetically engineered *ex vivo* to also express a resistance (Asp57+) MHC class II molecule. The thymus of the reconstituted mice -- carrying BM-derived cells that co-expressed both their own diabetogenic (non-Asp57) and the transfected Asp57 beta chain -- repopulated by the engineered BM cells, can restore an efficient negative selection and consequently the ability to delete T cells potentially auto-reactive to pancreatic beta cells. These diabetics will then be disease-free.

15. SUBJECT TERMS
Type 1 diabetes; autoimmunity; bone marrow; stem cells; histocompatibility

16. SECURITY CLASSIFICATION OF:			17. LIMITATION OF ABSTRACT	18. NUMBER OF PAGES	19a. NAME OF RESPONSIBLE PERSON USAMRMC
a. REPORT U	b. ABSTRACT U	c. THIS PAGE U	UU	39	19b. TELEPHONE NUMBER (include area code)

University of Pittsburgh
W81XWH-09-1-0742
Annual Report (09/28/2009 – 09/27/2010)
Table of Contents

       (published papers)

Background and Significance

Low levels of peripheral tissue-specific autoantigen (PTA) expression in immune cells have been implicated as one of the many means the immune system utilizes to ensure self-recognition and maintenance of tolerance. In central lymphoid organ, the thymus, PTA expressions were found to be restricted to epithelial cells within the medulla region; and at least some of them were regulated by the autoimmune regulator (*Aire*) gene. Animals with the *Aire* gene disrupted exhibit immune cell infiltration, as well as humoral response, to multiple peripheral solid organs, including the liver, the pancreas, and the stomach. It is conceivable that loss of PTA expression/presentation within the medulla could perturb the negative selection process of PTA-specific autoreactive T cells and crumple the central tolerant mechanism. Indeed, we have demonstrated conclusively that insulin-expression in medulllary thymic epithelial cells (mTECs) is essential to mediate islet beta cell-specific immune tolerance. ID-TEC mice with insulin deletion specifically in mTECs develop autoimmune diabetes spontaneously around three weeks after birth, due to T-cell mediated beta cell specific destruction. Intriguingly, when effector T cells were adoptively transferred to immune compromised *Rag1* knockout mice, only mild hyperglycemia were observed, even though islet infiltrations of immune cells from mild to severe levels were readily detected. Similar islet autoimmunity was observed in our thymus-transplantation model, in which ID-TEC thymi were harvested and transplanted under the kidney capsule of athymic nude mice. These data implicate the existence of protective peripheral mechanism that could effectively negate the actions of peripheral PTA-specific autoreactive T cells escaped thymic negative selection.

Like the thymus, PTA expressions were also found in the stroma of peripheral lymphoid organs, including the spleen and lymph nodes. Both bone marrow-derived antigen presenting cells and epithelial cells have been implicated in peripheral tolerance induction, though direct functional evidence in naive animals is still missing. As peripheral cells (such as bone marrow cells and epithelial cells) are more accessible compared to the thymus, understanding the roles of PTA expression in peripheral lymphoid in tolerance induction would have foremost impact on developing therapeutic regimen to cure autoimmune diseases, including type 1 diabetes. With this goal in mind, we set to develop animal models to investigate the roles of insulin expression in bone marrow derived antigen presenting cells in tolerant induction towards islet beta-cells. Two animal models are being generated to address these questions: the ID-DC line in which the mouse insulin 2 gene was specifically targeted and deleted in antigen presenting dendritic cells (DCs), and the ID-BMC line, in which insulin was deleted in all bone marrow derived antigen presenting cells, including macrophages, B-cells as well as DCs. Results from these models will help us to unravel the importance of specific antigen-presenting cell types in regulating insulin autoimmunity.

Experiments in Progress

1) Progress of animal breeding to establish the ID-BMC line.

To establish the ID-BMC line, a Vav-Cre transgenic line was generated in which the promoter/enhancer elements of the mouse *vav1* gene was used to drive Cre-recombinase expression in bone marrow progenitor cells. The Vav-Cre line was first crossed to *Ins1* knockout line, and then bred to Ins2-floxed: Ins1-null mice previously generated in the lab. Of note, the Vav-Cre transgenic line can only be maintained as hemizygous as pups homozygous for the transgene perish at embryonal stage. Through multiple rounds of breeding and genetic selection, we were able to setup breeding pairs with Vav-Cre:Ins2-floxed:Ins1-null/wt (male) and homozygous Ins2-floxed: Ins1-null (female) genotypes. As predicted from Mendel's law, our current chance to get ID-BMC pups (with Vav-Cre:Ins2-floxed: Ins1-null genotype) from these breeding pairs is about 25%. At present, we were able to obtain successfully a small number of ID-BMC founders, which will be used to replace the above Vav-Cre carriers in the mating setups, to increase our chances to obtain ID-BMC pups from 25% to 50%.

2) Progress of animal breeding to establish the ID-DC line.

To establish the ID-DC line, a DC-specific CD11c-Cre transgenic line was obtained from the Jackson Laboratory and was first crossed to *Ins1* knockout line, with an approach similar to that of obtaining the ID-BMC line. At present, we were also able to obtain a small number of ID-DC pups, which will be used as founders to get more ID-DC pups for the study.

3) Initial Characterization of Vav-Cre:iYFP mice.

To validate that the Vav-Cre transgene can efficiently target the loxP-tagged Ins2 gene in bone marrow-derived cells, we crossed the Vav-Cre line to the inducible Rosa-iYFP reporter line. In Rosa-iYFP mice, transcription of the yellow fluorescent protein (YFP) was blocked by a loxp-tagged neo cassette inserted between the universal Rosa26 promoter and the YFP coding sequence. Cre-mediated depletion of the floxed neo cassette will bring the YFP sequence physically adjoining the Rosa26 promoter and turn on YFP expression. Thus, the presence of YFP in special cells can reflect faithfully the expression pattern of the tissue-specific Cre transgene.
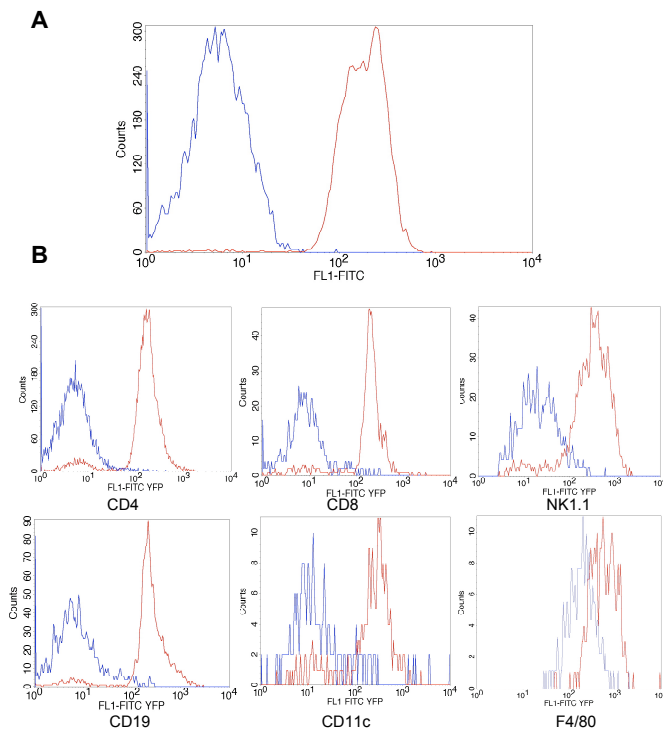
Figure 1. Characterization of Vav-Cre: iYFP mice. **A.** Peripheral blood samples were harvested and treated with red cell-lysis buffer and stained with anti-CD45 antibody. CD45+ cells were analyzed for YFP expression. Red line: Vav-Cre:iYFP; Blue line: Rosa-iYFP control. B. Splenocytes harvested from Vav-Cre:iYFP mice were stained with CD4, CD8, NK1.1, CD19 CD11c and F4/80 antibodies together with CD45 antibody analyzed by FACS for YFP expression (x-axis). Cells were gated for double positive of CD45+ and the antibody shown underneath each panel.

YFP expression in peripheral blood mononuclear cells (PBMCs) was first evaluated in Vav-Cre:iYFP mice. As shown in Figure 1A, almost all the PBMCs are YFP-positive, indicating high efficiency of the Vav-Cre transgene in hematopoietic lineages (**Figure 1A**), consistent with our previous results using Rosa-iLacZ as

5

reporter line. To further characterize the Vav-Cre expression in specific hematopoietic cell types, secondary lymphoid organs (including the spleen and the lymph nodes) were harvested and YFP expressions in specific cell types were characterized with FACS analysis. As shown in **Figure 1B**, YFP molecules are present in more than 95% of CD4+T cells, CD8+ T cells, B cells and NK cells. Of note, professional antigen presenting cells (APCs), including CD11c+ dendritic cells (DCs) and F4/80+ macrophages, also exhibit high percentage of YFP-positivity (~93% and 100%, respectively). Similar results were obtained from cells harvested from lymph nodes.
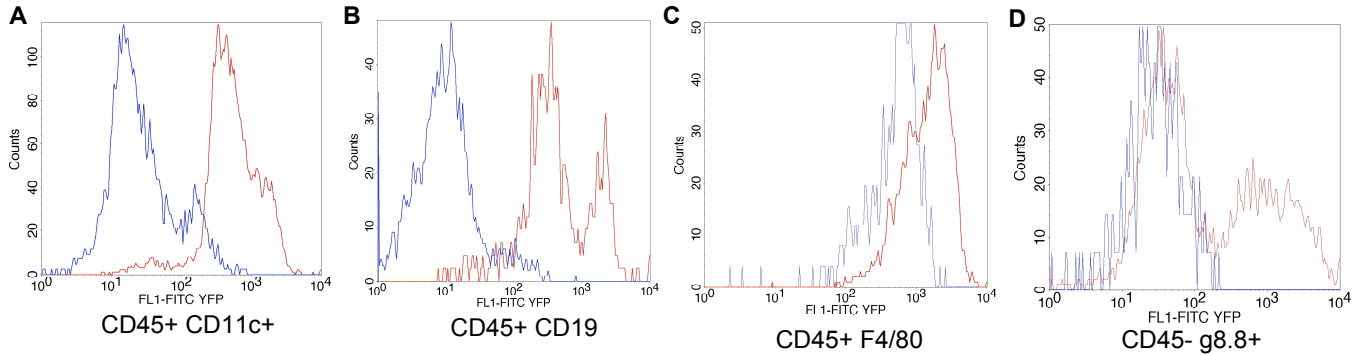

Figure 2. Characterization of YFP expression in the thymi of Vav-Cre:iYFP mice. Thymi harvested from Vav-Cre:iYFP mice were digested with colleagenase to single cell suspension. After CD90 magnetic bead-depletion of thymocytes, cells were further separated into CD45+ bone marrow derived and CD45- epithelial populations. CD45+ cells were stained CD11c, CD 19 and F4/80 antibodies, respectively; whereas CD45- cells were stained with g8.8 and Ly51. YFP expression in specific cell types (gated as labeled under each panel) was evaluated by FACS. Red line: Vav-Cre:iYFP; Blue line: Rosa-iYFP control.

YFP expression pattern in thymi harvested from the Vav-Cre:iYFP mice was also examined. Consistent with results from the periphery, Vav-Cre transgene can efficiently turn on YFP expression in thymic APCs (including DCs, macrophages and B cells). We also examined CD45- thymic stromal cells (**Figure 2A-2C**). About 65% of the CD45-
g8.8+ thymic epithelial cells are negative for YFP (**Figure 2D**). Further characterization of these cells showed that YFP-negative cells belonged to the Ly51 low compartment (data not shown), indicating that Vav-Cre is not expressed in thymic medullary epithelial cells. All in all, these data indicate that the Vav-Cre transgene can efficiently delete the floxed Ins2 gene in APCs derived from hematopoietic lineage in both central and peripheral immune organs.

3) Results from preliminary characterization of ID-BMC mice.

With the small number of ID-BMC mice obtained, we were able to do a number of experiments to characterize them preliminarily. First, we directly examine the efficiency of the Vav-Cre transgene mediating deletion of the floxed Ins2 gene. As shown in Figure 3A, Southern blot analysis of genomic DNA harvested from bone marrow progenitor cells of ID-BMC mice showed almost 100% deletion of the floxed Ins2 allele. However, RT-PCR analysis of thymi harvested from 6-week old ID-BMC mice showed that thymic insulin expression is largely intact in ID-BMC mice (**Figure 3B**), suggesting that within the thymus, the majority of the Ins2 transcripts observed are derived from mTECs. These animals are normoglycemic at 6-weeks, and we are closely monitoring their blood glucose levels on weekly basis.
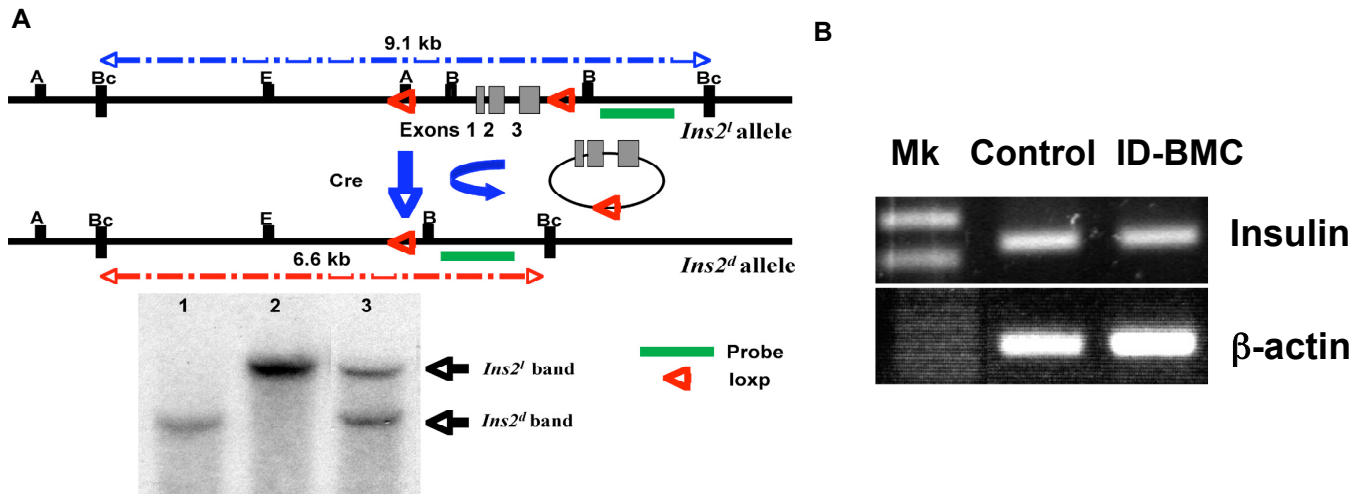

Figure 3. Characterization of ID-BMC mice: A preliminary study. A. Southern blot analysis of genomic DNA harvested from bone marrow progenitor cells of ID-BMC mice. *Upper panel:* Schematic drawing of the Ins2 floxed allele and the Ins2 deletion allele. Restriction endonucleases: A, AseI; Bc, BclI; B, BamHI; E, EcoRI. Cre mediated action will eliminate the Ins2 DNA fragment between the two flanking loxp sites, resulting a shorter fragment compared to the floxed allele (6.6kb vs 9.1kb) when genomic DNA samples were digested with BclI. Red triangle, loxp site; Green line, probe for Southern analysis. Lower panel: Southern blot showing the nearly total deletion of the Ins2-floxed allele in ID-BMC bone marrow cells (lane 1, upper band). Lane 2, DNA from bone marrow of homozygous floxed mice. Lane 3, DNAA harvested from bone marrow of heterozygous mice with one Ins2 deletion allele and one floxed allele. **B.** RT-PCR analysis of thymic insulin expression in ID-BMC mice. Mk. Molecular marker. Comparable levels of insulin expression were found in thymi of control (Ins2-floxed, Ins1-null) littermates and ID-BMC mice.

12. Use additional page(s) to present a brief statement of plans or milestones for the next quarter.

1) We have proved that the Vav-Cre transgene can efficiently target Cre-mediated deletion in all hematopoietic compartment, especially in antigen-presenting cells within both the primary and secondary lymphoid organs, but not in medullary epithelial cells. Our breeding scheme to generate both ID-BMC and ID-DC lines are successful and we have already obtained a small number of founder animals. These founder animals will enable us to get more ID-BMC and ID-DC mice for experimental purposes and speed up the study.

2) As predicted, the Vav-Cre transgene can efficiently mediate recombinant events in all cell types of the hematopoietic lineages. Especially, it enables high efficient deletion of insulin in antigen presenting cells of bone marrow origin in both central and periphery organs. Such feature will allow us to investigate the immunologic importance of insulin ectopic expression bone marrow derived APCs in mediating self-tolerance.

3) Our preliminary results from a small number of ID-BMC animals suggest that bone marrow-derived APCs are not the major source of thymic insulin transcripts. No major change of levels of insulin expression is detected, even though near total deletion of the floxed Ins2 alleles was achieved in all bone marrow derived cells. We are in the process of further evaluate insulin autoimmunity in these animals.

Background and Significance

Peripheral tissue-specific antigen (PTA) expression in immune cells of the central or peripheral lymphoid organs has been implicated in establishing and maintaining immune tolerance towards self. We and other have demonstrated conclusively that abrogation of a single PTA in medullary thymic epithelial cells (mTECs) is sufficient to trigger tissue-specific autoimmunity. Recently, attentions have also been drawn to the non-haematopoietic stromal compartments in peripheral lymphoid organs, as above-noise levels of PTA transcripts were detected. Stromal cell types expressing different surface markers or transcription factors were shown to possess the properties of PTA-production, and their roles in modulating peripheral tolerance towards different tissues and organs were heavily debated. Anderson and colleagues isolated EpCAM+, MHC II+, Aire+ eTACs (extrathymic Aire-expressing cells) and showed that a diverse array of PTAs were expressed in these cells and they were capable to interact with and delete autoreactive T cells. In contrast, Engelhard's group from University of Virginia identified a population of gp38+MHCII+ lymph node stromal cells (LNSC) that can directly express and present multiple PTAs. Interactions between autoreactive cytotoxic CD8+ T cells specific to a melanoma-specific antigen (MSA) with MSA-expressing LNSCs induce programmed cell death of the T cells. Intriguingly, Turley's group from Harvard University reported recently that more than one stromal cell types in the lymph nodes possessed the PTA-expressing, tolerogenic induction properties; and that levels and diversity of PTA expression in the stroma are responding to environmental cues, such as virus infection and inflammation. Nevertheless, these new findings suggest the existence of another checkpoint mechanism in the immune system to maintain self-tolerance.

In this quarter, we continued to characterize the ID-BMC and ID-DC mouse models as mentioned previously. In addition, we also took advantage our Aire-Cre transgenic line to examine the presence of Aire-expressing cells in the periphery. Specifically, we crossed Aire-Cre transgenic mouse to RosaYFP reporter mouse to generate the Aire-Cre:RosaYFP. As mentioned previously, YFP expression was blocked by a stopper sequence that flanks the constitutively active Rosa26 promoter and the YFP coding sequence in RosaYFP mouse. Cre-recombinase molecules translated from the Aire-cre transgene could efficiently delete the stopper sequence, and acted as a molecular switch to permanently turn on YFP expression. Thus, YFP can be used as a molecular tracer to truthfully record the developmental history of the Aire-expressing cells. Here, we reported our findings within the 1st quarter.

Experiments in Progress

1) Characterization of ID-BMC mice.

We have shown from a small number of ID-BMC animals that bone marrow-derived antigen-presenting cells are not the major source of thymic insulin transcripts. No major change of levels of insulin expression is detected, even though near total deletion of the floxed Ins2 alleles was achieved in all bone marrow derived cells. ID-BMC mice remain euglycemic for more than 16 weeks; and we did not observe any incidence of hyperglycemia, in striking contrast to the 100% penetration of spontaneous diabetes observed in our mTEC-specific insulin-deletion ID-TEC colony three weeks postnatal. Furthermore, we did not observe any CD4+ T-cell infiltration or insulitis in the pancreata of ID-BMC mice, indicating the absence of any islet autoimmunity (Figure 1). We are currently developing in vitro assays to directly examine the presence/absence of anti-insulin specific T cells in ID-BMC mice.
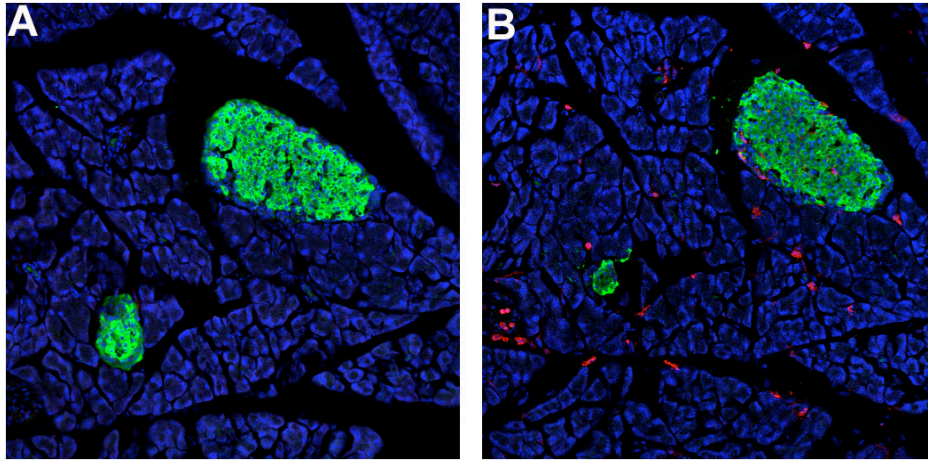
Figure 1. Immunohistochemical analysis of pancreata harvested from ID-BMC mice. Pancreata harvested from 12-week old ID-BMC mice were fixed with 4% paraformaldehyde. 5um cyrosections were stained with anti-insulin (green), anti-CD4 (red, **A**), and anti-CD45 (red, **B**) antibodies. Although CD45+ residue immune cells are readily detectable, no CD4+ T-cells was observed infiltrating the pancreas.

2) Characterization of the ID-DC lines.

With the small number of founder animals, we were able to expand a limited number of ID-DC mice. Similar to the ID-BMC line, all the ID-DC mice remain euglycemic for more than 8-weeks. We are currently expanding the colony to further characterize the animals both *in vitro* and *in vivo*.

3) Characterization of the Aire-Cre:YFP mice.

As the first step, we harvested solid organs from the Aire-Cre:YFP mice and examined the YFP expression by histology. Consistent with our previous results, no co-staining of YFP signal and insulin was observed, indicating that Aire-Cre was not expressed in insulin-secreting pancreatic beta-cells (Figure 2). Interestingly, we did observe YFP positive cells in the spleen (Figure 2, spleen section on the top), consistent with previous findings of the presence of PTA-expressing cells. Interestingly, YFP positive cells were not detected in the white pulp region, where active immune humoral and cellular responses occur, but were largely present in the marginal zone bordering the white pulp. Such geometrical location are consistent with a tolerogenic role of Aire-expressing cells where naive T cells were first interrogated by self-antigens before they migrate into white pulp to elicit active immune response. Sparse YFP positive cells were also observed in a number of solid organs and tissues, including the lung, kidney, stomach and the intestines, but not observed in brain or heart (Figure 2). Morphological examination suggests that most of them are epithelial cells, and there was no clonal clusters, indicating that the YFP positive cells are not necessarily from the same ancestral lineage. Indeed, it was recently shown that Aire-mediated expression of PTA was also observed in the epithelium of the thyroid, suggesting that random PTA-expression is a general property of certain epithelial cells. However, its immunologic significance in regulating self-tolerance remains to be examined.
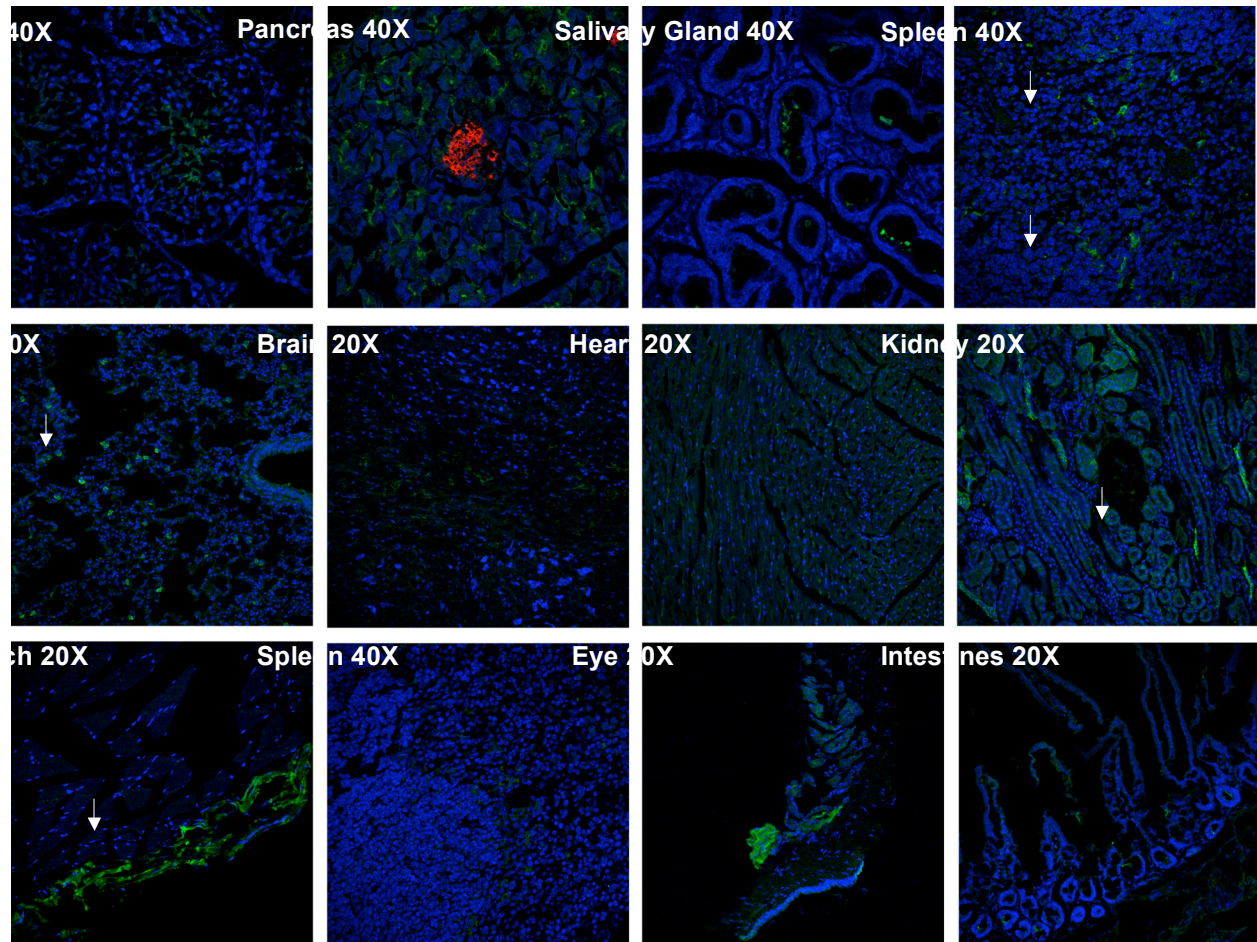
Figure 2. Immunohistochemical analysis of patterns of Aire-Cre expression. Solid organs harvested from Aire-Cre:RosaYFP mice were fixed in 4% paraformaldehyde and cyrosections of 5um thick were stained with rabbit anti-GFP polyclonal antibodies (green, all the slides), as well as anti-insulin antibody (the pancreas section). White arrows indicate the YFP-positive cells in the spleen, lung, stomach and kidney.

Another interesting findings in our histological characterization of the Aire-expression pattern is the presence of YFP signal in mature spermatozoa, but not in immature spermatids. The presence of YFP signal in the male reproduction system raised the question: how Aire-Cre transgene retain its specificity of mTEC-specific Cre expression if the transgene is active in the sperm. One potential explanation is that the tight compaction of chromosomal DNA in mature sperm is resistant to Cre-mediated deletion of the loxp-flanking DNA element. Furthermore, the small amount of Cre-recombinase protein introduced into the fertilized egg is insufficient to mediate efficient homologous recombination.

4) YFP expression in Aire-Cre:RosaYFP thymus.

We also examine patterns of YFP expression in Aire-Cre:RosaYFP stroma. CD45-EpCAM+MHCII+ thymic epithelial cells (TECs) were harvested and examined by FACS analysis. As shown in Figure 3, about 68% of the TEC cells are YFP-positive, consistent with our observation that 60-70% of TECs isolated in our protocol are mTECs. These results suggest that our Aire-Cre:RosaYFP model can efficiently label all the mTECs in the thymus. Interestingly, we also observed ~8% of thymic CD11c+ dendritic cells (DCs) are YFP positive. Indeed, low levels of Aire transcripts were previously detected in thymic DCs. Alternatively, these YFP signals were derived from engulfing of mTEC components by thymic DCs for cross-presentation. Nevertheless, our Aire-Cre:RosaYFP can faithfully reproduce the pattern of Aire expression pattern in the thymus, and can efficiently label all the mTECs.

Pattern of YFP expression in Aire-Cre: RosaYFP thymic stroma
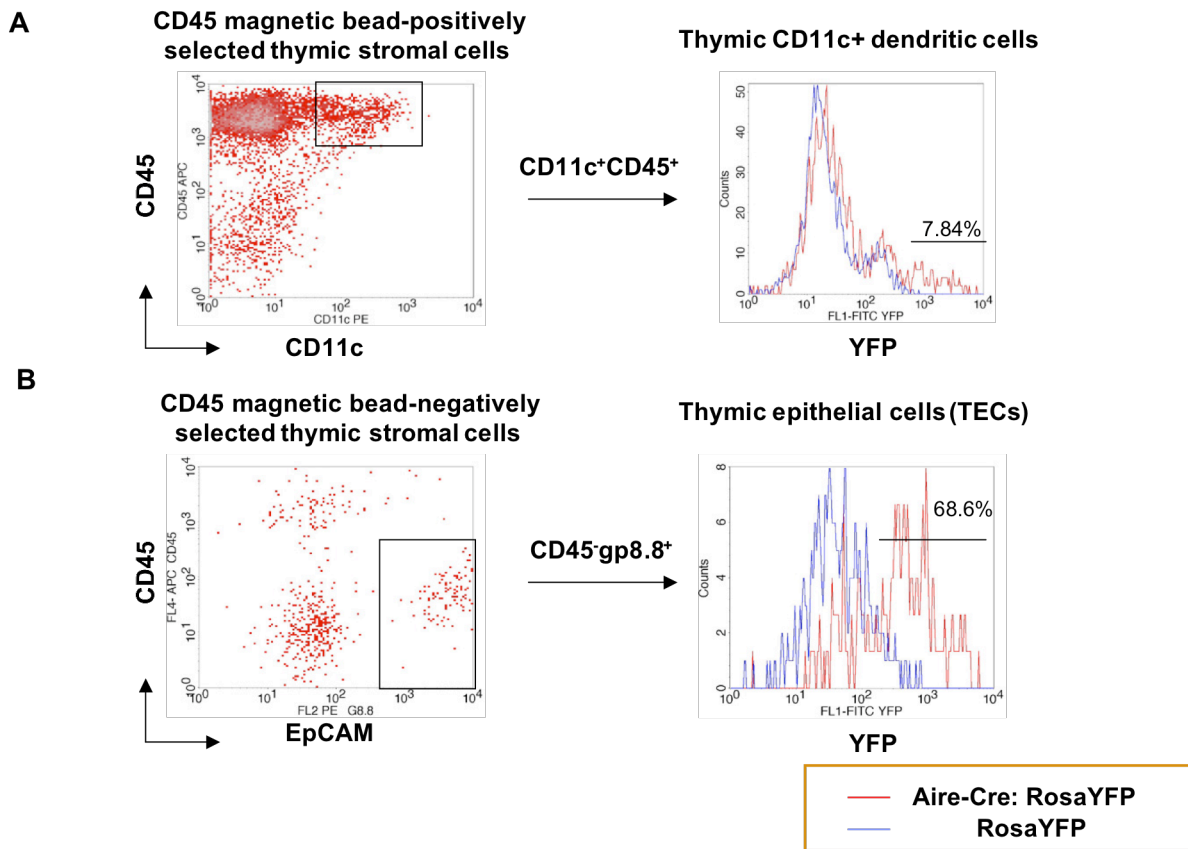
Figure 3. Aire-expressing cells in thymic stroma. Aire-Cre:RosaYFP thymi were harvested and separated into single cells via collagenase digestion, followed by CD90 magnetic bead-depletion of thymocytes. The negatively selected cells were further separated by CD45 antibody conjugated magnetic beads into the CD45+ bone marrow-derived cells (A) and the CD45- epithelial cell population (B). As shown in Panel B, about 60-70% of TECs are YFP positive, which is consistent with the 2:1 mTEC to cTEC ratio, which we normally observed during TEC isolation (with Ly51 and UEA-1). We also routinely found a small percentage of thymic dendritic cells (CD4-CD45+CD11c+) that are YFP positive (~7-8%).

REFERENCES

1. Gardner JM, Devoss JJ, Friedman RS, Wong DJ, Tan YX, Zhou X, Johannes KP, Su MA, Chang HY, Krummel MF, Anderson MS (2008). Deletional tolerance mediated by extrathymic Aire-expressing cells. Science. 321(5890):843-7.

2. Cohen JN, Guidi CJ, Tewalt EF, Qiao H, Rouhani SJ, Ruddell A, Farr AG, Tung KS, Engelhard VH (2010). Lymph node-resident lymphatic endothelial cells mediate peripheral tolerance via Aire-independent direct antigen presentation. J Exp Med. 207(4):681-8.

1. Fletcher AL, Lukacs-Kornek V, Reynoso ED, Pinner SE, Bellemare-Pelletier A, Curry MS, Collier AR, Boyd RL, Turley SJ (2010). Lymph node fibroblastic reticular cells directly present peripheral tissue antigen under steady-state and inflammatory conditions. J Exp Med. 207(4):689-97.

12. Use additional page(s) to present a brief statement of plans or milestones for the next quarter.

1) We expanded our studies on ID-BMC mice during this quarter, and did not observe any pathological signs of diabetes in these animals. Furthermore, no CD4+ T cell infiltration was observed in ID-BMC pancreas, suggesting that deletion of insulin in bone marrow derived antigen presenting cells are not essential to establish immune tolerance towards islet beta cells.

2) We have also established an Aire-Cre:RosaYFP animal model, which can faithfully reproduce the expression patterns of the Aire gene in the thymus. Our immunohistochemical characterization of the YFP expression patterns in peripheral tissues and solid organs revealed the interesting finding that Aire is also sparsely expressed in epithelial cells of a variety of tissues and organs.

3) In the next quarter we will use now the Aire-Cre:RosaYFP animals as a useful tool to isolate and characterize PTA-expressing cells in both the central and peripheral lymphoid organs, which will significantly facilitate our understanding of the underlying mechanisms of establishing and maintaining immune tolerance towards self.

Our third quarterly scientific progress report for the initial year of our project (03/28/10 – 06/27/10) was waived since a detailed report was presented at the Diabetes and Chronic Disease Product Line Review on June 15, 2010. We are including a summary of the slides presented there.

Slide 1: Safe Gene Therapy for Type 1 Diabetes — Dr. Massimo Trucco, Principal Investigator. Product Line Review (PLR) Meeting, Diabetes and Chronic Disease: Filling the Gaps, 15 June 2010. 28 Sept 09 – 27 Oct 11, $3,604,000.00, CSI

Slide 2: Military relevant issue to be solved — Insulin-Dependent Diabetes Mellitus (Type 1 Diabetes). Human islet of Langerhans with insulitis, Trucco et al. CRC Reviews 9:201, 1989

Slide 3: Military relevant issue to be solved — Insulin-Dependent Diabetes Mellitus (Type 1 Diabetes). Human islet of Langerhans with insulitis, Trucco et al. CRC Reviews 9:201, 1989

Slide 4: Solution — Epithelial Thymus Cells. Positive and Negative Thymic Selection. Trucco & Giannoukakis Gene Therapy 12:553, 2005

Slide 5: Project Description

Slide 6: Project Description

Slide 1 — Project Description

Project Description

Endogenous C-Peptide in treated NOD Mice

Serum C-peptide (ng/ml) — y-axis: 0, 2, 4, 6, 8, 10, 12, 14, 16, 18

Legend: 0 min, 10 min

Categories: Untreated #1, Untreated #2, Treated #1, Treated #2

Slide 2 — Project Description

Project Description

$Ins1^{-/-}$ X $Ins2^{kl}$ $Ins1^{-/-}$ X Cre

$Ins1^{-/-}$ $Ins2^{kl}$ X $Ins1^{-/-}$ Cre

$Ins1^{-/-}$ Cre $Ins2^{kl}$

Aire-Cre
(Medullary epithelial cells in thymus)

Thymus

$Ins1^{-/-}$ Aire-Cre   Ins2

Islet β-cells

$Ins1^{-/-}$ Aire-Cre   Ins2

Fan et al. *EMBO J.*, 28:2812, 2009

Slide 3 — Project Description

Project Description

Control   ID-TEC *

Glucagon + Insulin + Nucleus

Day 1

Blood glucose (mg/dl) — 0, 100, 200, 300, 400, 500, 600, 700

Legend: Control, ID-TEC, ID-TAPC

Postnatal Days — 10 15 20 25 30 35 40 45

Day 17

*ID-TEC = insulin-deprived thymic epithelial cells

Fan et al. *EMBO J.*, 28:2812, 2009

Slide 4 — Validation Strategy

Validation Strategy

Transplantation of ID-TEC thymi into nude mice.

Aire-Ins2   Thymus   2-deoxyguaosine

CD4+

CD8+

T-cell Development

Fan et al. *EMBO J.*, 28:2812, 2009

Slide 5 — Validation Strategy

Validation Strategy

Lymph nodes   Spleen

CD4+

CD8+

WT   ID-TEC

ID-TEC   ID-TEC

Fan et al. *EMBO J.*, 28:2812, 2009

Slide 6 — Research/Development Timeline

Include detailed timeline/Gantt chart

Research/Development Timeline

Milestone #1: To demonstrate whether BM derived cells carrying the H2 molecule able to confer resistance to type 1 diabetes (I.E., our "treatment") need to also express self-antigens to properly present them and complete negative selection, or have to capture them from other cells for cross presentation. The strategy in which T1D can be reverted by substituting a "diabetes-susceptible" class II MHC beta. — **May 2010**

Milestone #2: To test the efficacy of the treatment in terms of its ability to allow the regenerative capabilities of the diabetic pancreas to recover sufficient insulin production for controlling the animal glycemia in new-onset diabetic NOD mice, while characterizing the immune scenario that favors this regeneration (e.g., regulatory T-cell expansion). — **September 2010**

Milestone #3: To ascertain the efficacy of engraftment and repopulation capabilities of the engineered hematopoietic precursor cells, following non-radiation based pre-conditioning. A combination of two antibodies (anti-c-kit and anti-CD52) will be used instead. — **December 2010**

Milestone #4: To substitute non-viral minicircle DNAs for retroviruses as the vectors for transfecting the protective histocompatibility H2 I-A beta chain transgene into enriched autologous BM hematopoietic cell precursors. — **May 2011**

Milestone #5: To re-program differentiated pancreatic exocrine cells of autoimmunity-free NOD mice into cells that "closely resemble beta cells". — **September 2011**

15

Slide 13 — Successes to Date

Successes to Date

To target specific types of antigen presenting cells in the thymic stroma,
three transgenic animal lines were generated:

CD11c-Cre   Vav-Cre   Aire-Cre

Thymic dendritic cells   Macrophages   Thymic medullary epithelial cells

---

Slide 14 — Intellectual Property / Publications Deriving from this Project

Intellectual Property / Publications Deriving from this Project

•Confidentiality Agreements:
   Materials Transfer Agreements were signed between the University of Pittsburgh and a number of other Institutes:
   –National Institute of Health (Dr. Hodes).
   –University of Calgary, Canada (Dr. Santamaria).
   –Washington University, St. Louis (Dr. Moley)

•Patents Filed:
   –None at present, but we are certainly aware of the possibilities when our research move along further.

Slide 15 — Intellectual Property / Publications Deriving from this Project

Intellectual Property / Publications Deriving from this Project

•List all Publications deriving from the project:

Fan Y, Rudert WA, Grupillo M, He J, Sisino G and Trucco M.
   "Thymus-specific deletion of insulin induces autoimmune diabetes".
The EMBO Journal 28: 2812-2824, 2009.

   Feature article of the issue.
   Selected at NIH as Faculty of 1000 exceptional paper with F1000 factor 9.0
   Selected for the 2010 Senior Vice Chancellor's Research Seminar Pitt. Univ.

Two manuscripts are currently under preparation:

Ecotopic insulin expression in bone marrow derived antigen presenting cells is not indispensable for maintaining immune tolerance towards beta cells.

Self-tolerance mediated by peripheral tissue specific antigen expression: the Aire experience.

Slide 16 — Project Funding

Project Funding

Current Budget	Expended Funds
$ 2,007,693	$ 392,384
	(out of $ 1,561,796 received to date)

Other Funding if applicable

NIH,   1 U01 DK61058-01
Title: Prediction and Prevention of Type 1 Diabetes
Annual Direct Costs: 09/01/09 -- 08/31/10; $ 315,019
      Entire Period: 09/01/09 - 08/31/14; $ 2,519,975

Henry Hillman Endowed Chair to M. Trucco
      $ 382,360

Cochrane Webber Endowment to Yong Fan
      $ 25,000

Slide 17 — Additional Project Information

Additional Project Information

Lab/Company/Group: University of Pittsburgh
Principal Investigator: Dr. Massimo Trucco
Government COR: Mr. Robert Read
Government Project Officer: Stacy Zimmerman
Contract Instrument: Grant
Period of Performance: 28 Sept 09 – 27 Sept 11
Contract Specialist: Ms. Nita Bourne
EDMS# : 4235
Contract #: W81XWH0910742

Background and Significance

In addition to pancreatic islets, low levels of insulin expression were found in a number of tissues and organs, including but not limited to the thymus, the brain, the salivary glands, the testis and the bone marrow. Although such extrapancreatic insulin production has been implicated in regulating many biological processes, such as maintaining metabolic and neuroendocrinological homeostasis under either physiological or pathological conditions, experimental evidence supporting these claims are mostly missing. We have a long interest in understanding the roles of insulin expression in cells of immune organs, and their implication in type 1 diabetes etiology. As described in previous reports, our ID-TEC animal model, in which insulin expression in medullary epithelial cells of the thymus (mTECs) is specifically targeted and depleted, demonstrated conclusively that thymic insulin production, albeit at low levels, is essential to establish adaptive immune tolerance of islet beta cells by eliminating insulin-specific autoreactive T cells through central negative selection mechanisms. Interestingly, insulin expression in immune-relevant organs is not restricted to epithelial cells of the thymic medulla. The presence of insulin transcripts in bone marrow derived antigen presenting cells have been reported by a number of groups. Taking advantage of the Aire-Cre:Rosa-YFP reporter line developed in our laboratory, we were able to identify at least two types of cells with antigen-presenting capability (expressing MHC II molecules) in secondary lymphoid organs: the $CD45^+CD11c^{int}MHCII^+$ cells in the spleen and the $CD45^-MHCII^+$ cells in stroma of lymph nodes (as reported in our third quarterly scientific report).

As reported in the previous quarters, we had generated a number of animal models, including the insulin deletion in bone marrow derived cells line (ID-BMC) and the insulin deletion in dendritic cells line (ID-DC), to investigate the immunologic significance of insulin expression in bone marrow derived antigen presenting cells. In this quarter, we continued our characterization of the ID-BMC and ID-DC lines, and conclude that depletion of insulin expression in antigen presenting cells of bone marrow origin is not sufficient to induce anti-insulin autoimmune response. In addition, we successfully introduced the autoimmune diabetes susceptible $H2^{97}$ MHC alleles from the NOD mice into the ID-DC lines, to evaluate the potential roles of insulin expression in DCs in preventing uncontrolled expansion of autoreactive T cells arisen from the faulty thymic negative selection. We will also present our results of initial characterization of these mice in this quarterly report.

Results of Experiments in Progress

1) Characterization of ID-BMC mice

As previously described, ID-BMC mice were born healthy with no obvious physiologic abnormalities, and did not show any sign of dysregulation of glycemic control throughout their lifespan (Figure 1, *left panel*). Compared with littermate controls, ID-BMC mice display normal response to glucose challenge, and normal insulin sensitivity, suggesting that there are no abnormalities in glucose metabolism and islet function (Figure 1, *right panel*). Consistently, normal islet structure and insulin production were observed in pancreata harvested from ID-BMC mice. We did not observe any damaged islets nor islets infiltrated with immune cells (a.k.a. insulitis), indicating the absence of anti-islet autoimmunity. Furthermore, compared with controls, no above the background levels of insulin-specific autoreactive T cells was observed in ELISPOT assays of ID-BMC splenocytes, using insulin or its peptides as stimulants. Thus, elimination of insulin expression in bone marrow derived antigen presenting cells is insufficient to break down immune tolerance towards insulin to trigger anti-islet autoimmunity.

Normal Blood Glucose Levels

Intraperitoneal Glucose Tolerance Test

Minutes after glucose injection (2g/kg)
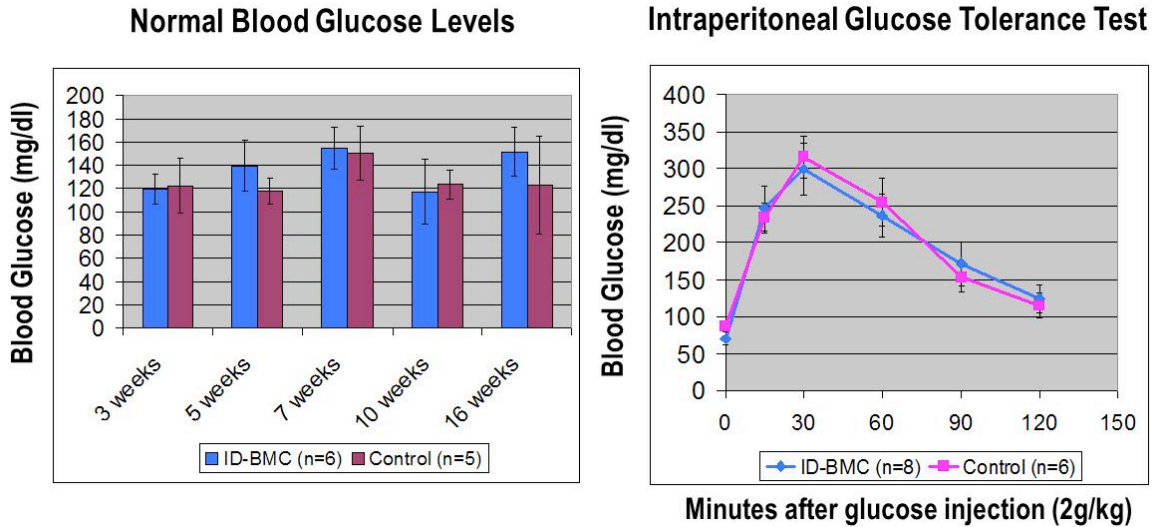
Figure 1. ID-BMC mice can maintain normal glucose homeostasis. *Left panel*, ID-BMC mice display normal levels of blood glucose levels, as compared with controls. *Right panel*, 16-week old ID-BMC mice were fasted overnight, and challenged with intraperitoneal injection of glucose (2g/kg body weight). No difference was observed between ID-BMC mice and controls, indicating that ID-BMC mice can efficiently maintain glucose homeostasis.

2) Insulin expression in plasmacytoid dendritic cells (pDCs) within the spleen.

As low levels of Aire gene expression were was found in bone marrow-derived CD11c+ dendritic cells within the thymus, we took advantage of the fact that Aire-Cre transgene can faithfully recapitulate the endogenous Aire gene expression pattern and investigated whether a similar $Aire^+$ $CD11c^+$ DC population were present in secondary lymphoid organs. Aire-Cre transgenic mice were crossed to reporter RosaYFP mice to generate the Aire-Cre:RosaYFP line. Indeed, about 1% of the CD45+ splenocytes, with the molecular signature of tolerogenic, plasmacytoid DCs ($CD11c^{int}$, $MHCII^+$), are YFP+ (Figure 2, *left panel*). Interestingly, qPCR analysis of insulin gene expression revealed that insulin transcripts are predominantly present in $CD11c^{int}YFP^+$ of cells, but not in $CD11c^{high}YFP^-$ DCs (Figure 2, *right panel*), indicating that, unlike thymus, insulin expressions in the spleen are largely restricted to $Aire^+$, plasmacytoid DCs of bone marrow origin.
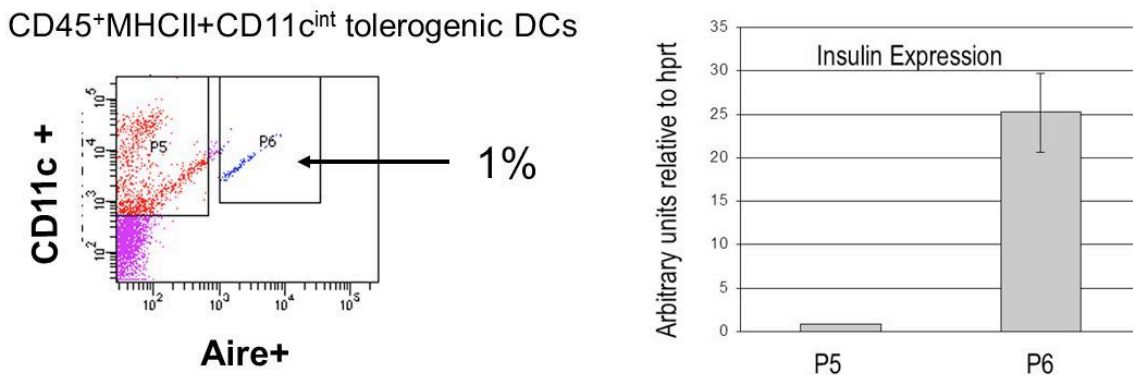
Figure 2. Insulin is expressed in $Aire^+MHCII^+CD45^+CD11c^{int}$ plasmacytoid DCs in the spleen. *Left panel*, FACS analysis showed that about 1% of the CD45+ splenocytes (box marked with P6) express Aire and intermediate levels of CD11c, the molecular signature of tolerogenic plasmacytoid DCs. *Right panel*, qPCR analysis of insulin expression levels in classic $CD11c^{high}$ DCs (P5) and plasmacytoid, Aire+ DCs (P6), showing that insulin is predominantly expressed in Aire+ pDCs in the spleen.

18

3) **Characterization of ID-DC and ID-DC-H2g7 mice.**

To further investigate the function of insulin-expression in Aire^{+}CD11c^{int} DCs in the spleen, we crossed transgenic mice expressing Cre-recombinase under the CD11c promoter (CD11c-Cre) to Ins2$^{l/l}$:Ins1$^{d/d}$ mice to generate ID-DC mice, as previously described. Similar to ID-BMC mice, ID-DC mice remain euglycemic throughout life, with no signs of compromised glucose metabolism or islet autoimmunity (data not shown). As both ID-BMC and ID-ADC are under C57BL/6 background with autoimmune diabetes resistant MHC (H2b haplotype), which can efficiently present autoantigens within the thymic medulla to mediate central negative selection, autoreactive T cells with high-affinity to islet autoantigens were proficiently eliminated within the thymus. Thus, under conditions of effective thymic negative selection, deletion of insulin expression in tolerogenic DCs in the periphery will not induce anti-islet autoimmunity.

To examine the immune tolerogenic roles of insulin expression in Aire^{+}CD11c^{int} DCs under faulty central negative selection conditions, we introduced the autoimmune diabetes-susceptible H2^{g7} MHC alleles of the non-obese diabetic (NOD) mice to ID-DC mice through multiple rounds of breeding with B6-H2^{g7} congenic mice to generate ID-DC-H2g7 mice. ID-DC-H2g7 mice displayed similar levels of blood glucose as non-Cre littermate controls (Figure 3, *left panel*). As well, no difference of glucose metabolism was observed when challenged with intraperitoneal glucose injection (Figure 3, *right panel*), suggesting normal islet function.

Figure 3. Normal glucose metabolism in ID-DC-H2g7 mice. Left panel, ID-DC-H2g7 animals remain euglycemia. Right panel, Intraperitoneal glucose tolerance test (IPGTT). ID-DC-H2g7 mice display normal tolerance to glucose challenge, as compared with controls.

Plans or milestones for the next quarter:

1) Our results from characterization of ID-BMC mice clearly demonstrated that depletion of insulin in bone marrow derived antigen presenting cells is not sufficient to breach either central or peripheral immune tolerogenic mechanisms in animals w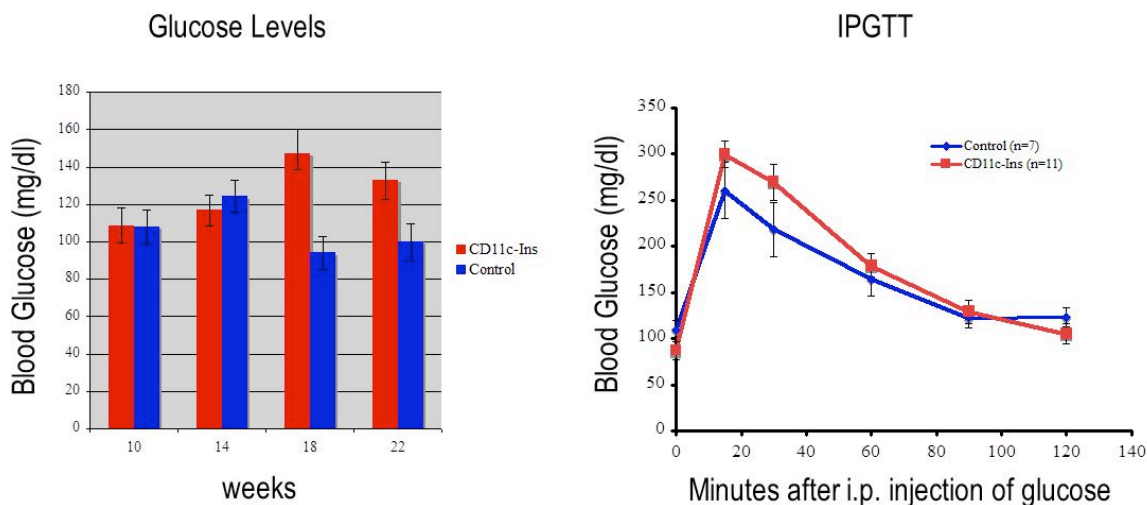ith autoimmune diabetes-resistant MHC. Our data also emphasize the dominant roles of central mechanism in establishing adaptive immune tolerance towards pancreatic beta cells. Thus, our focus in the future should be shifted to the roles of insulin expression in secondary lymphoid organs in preventing clonal expansion of insulin-specific autoreactive T cells which escaped negative selection.

2) We were able to identify a population of plasmacytoid DCs in the spleen which express both Aire and insulin. Further characterization of this population will allow us to explore the possibility of using these cells to strengthen peripheral tolerance to insulin, which might lead to development of individualized therapeutic vaccines to prevent insulin autoimmunity.

3) Although our initial characterization of the ID-DC-H2g7 mice did not display any abnormalities of islet function at physiological levels, we will investigate whether these animals display any anti-islet autoimmunity in the next quarter.

KEY RESEARCH ACCOMPLISHMENTS:

1. We have successfully generated and characterized the ID-BMC animal model in which insulin expression is abrogated only in bone marrow derived cells. We further demonstrated that the absence of insulin in bone marrow cells is not sufficient to induce autoimmune diabetes, thus, emphasize the dominant roles of central mechanism in T1D etiolgoy.

2. We have identified two insulin-expressing stromal cell types in secondary lymphoid organs, and we will explore their therapeutic potency to strengthen peripheral tolerogenic mechanism to counteract preexisting faulty thymic negative selection conditions.

3. We have successfully generated ID-DC and ID-DC-H2g7 animals, in which insulin expression is specifically knocked out in both classic and tolerogenic dendritic cells. These animals will allow us to dissect further the interactions between central and peripheral immune mechanisms in establishing/regaining insulin tolerance.

REPORTABLE OUTCOMES:

Manuscripts (5 publications)

1. Lu C, Kumar PA, **Fan Y**, Sperling MA, Menon R (2010) A novel effect of GH on macrophage modulates macrophage-dependent adipocyte differentiation. *Endocrinology* 151 (5): 2189-2199.

2. Perdomo G, Kim DH, Zhang T, Qu S, Thomas EA, Toledo FG, Slusher S, **Fan Y**, Kelley DE, Dong H (2010). A role of apolipoprotein D in triglyceride metabolism. *Journal of Lipid Research* 51: 1298-1311.

3. Mavalli M, DiGirolamo D, **Fan Y**, Riddle R, Campbell K, Sperling M, Frank S, Bamman M, Clemens T (2010). Distinct growth hormone receptor signaling modes control skeletal muscle development and insulin sensitivity. Manuscript accepted for publication in the *Journal of Clinical Investigation*. *J Clin Invest.* 2010; doi:10.1172/JCI42447.

4. Trucco M (2010). Beta-cell regeneration: from science fiction to challenging reality. *Pediatr Diabetes* 11(5):292-5.

5. Trucco M (2010). Gene-environment interaction in type 1 diabetes mellitus. *Endocrinol Nutr.* 56 Suppl 4:56-9.

CONCLUSION:

The conclusions from the current year of funding are that we demonstrate conclusively the dominant roles of thymic insulin expression in establishing adaptive immune tolerance towards islet beta cells of the pancreas. Ablation of insulin expression in bone marrow derived antigen-presenting cells will not induce autoimmune diabetes. We also identified two types of insulin-expressing stromal cells with antigen-presenting capability in the stroma of secondary lymphoid organs, which might play roles in maintaining peripheral islet beta cell tolerance under central defective conditions.

The So What Section:

What are the implication of this research?

Diabetes affects 16 million Americans and roughly 5-15% of all cases of diabetes are type 1 DM. It is the most common metabolic disease of childhood, and physicians diagnose approximately 10,000 new cases every year. Type 1 diabetes is associated with a high morbidity and premature mortality due to complications. The annual cost from diabetes overall exceeds $100 billion, almost $1 of every $7 dollars of US health expenditures in terms of medical care and loss of productivity.

What are the military significance and public purpose of this research?

As the military is a reflection of the U.S. population, improved understanding of the underlying etiopathology of T1D will facilitate the development of potential therapeutics to prevent the onset of the disease or the development of diabetic complications among active duty members of the military, their families, and retired military personnel. Finding a cure to T1D will provide significant healthcare savings and improved patient well being.

Perspective

Beta-cell regeneration: from *science fiction* to challenging reality

Type 1 diabetes is due to an autoimmune reaction directed against the pancreatic beta cells. Since some regenerative capabilities of the endocrine pancreas have now been quite well documented, and recent research has shown that human stem cells can be derived from embryos or from genetically engineered somatic cells, is it practical or even possible to combine these lines of research to more effectively treat young diabetic patients? The recently published paper of Pedro Herrera and his group (1) inspires a number of considerations that might help to properly answer this question, while bringing to mind unforgettable scenes from a popular 90's film. Herrera's results show that after near-total ablation of beta cells in the endocrine pancreas, some new beta cells are actually generated. However, these new beta cells originate from already existing alpha cells, rather than from preexisting beta cells or from other precursor cells.

> *Metallic drops, warmed by the sparks of melting iron, quiver and flow on the ground like quicksilver. They coalesce, and together they expand, change conformation, and eventually assume their final shape: it's T-1000, the liquid metal-based robot in the famous movie ''Terminator 2'' directed by James Cameron. The T-1000 is the nemesis of the T-800, the other, more conventional robot, sent back in time as mankind's savior. The task for the T-800 is quite difficult, since the T-1000 seems to be indestructible: Even after enduring tremendous damage, it can easily reassemble, repair, and finally regenerate itself, quickly resuming its original form.*

Fortunately for us, we do not have to be overly envious of the T-1000. Once damaged, parts of the human body also have the ability to repair, reassemble, and regenerate themselves, ultimately resuming their original conformations. With the exception of only a few tissues, our cells can be replaced fairly quickly and regenerate into functional tissues. Perhaps we

should not be surprised, then, that the endocrine pancreas is capable of functional regeneration, given adequate time and the appropriate physiological conditions. However, the nature of the requisite beta cell precursors, how they function, where they are physically located, and what influences them to regenerate the correct missing tissue, are all questions still awaiting definitive answers.

The 'stem cell' is, by definition, the one cell capable of duplicating itself and while maintaining its undifferentiated status, could also originate a progeny that differentiate into one or more different final products that are physiologically defined by their specific functions. Proceeding through the differentiation pathway, stem cells can be categorized as totipotent, pluripotent, multipotent, oligopotent, and unipotent, depending upon all their possibly irreversible, progressively acquired characteristics. Twins can actually develop from the same zygote, if its derived cells are properly separated very early in the embryological process. Although then, the vertebrate zygote might be considered the preeminent totipotent stem cell, it continues to divide to form the final individual: a mixture of similar, but not identical, daughter cells. Since we do not know yet which specific markers characterize the totipotent cell, we also do not know whether totipotent cells are still preserved, once the various tissues begin to differentiate into organs. If they are, how long could they continue to be functional? Intuitively, we can argue that precursors of some kind should still be present and active within the body indefinitely, because even elderly people are able to repair their damaged tissues. However, we still do not know the number of these regenerative precursors, where they may be hiding, and which level of differentiation they have already achieved.

Paraphrasing what I wrote some years ago (2), I would argue that a system based on a single regenerative center, serving all the peripheral needs, would be quite inefficient. If this were the case, even if an 'S.O.S.' transmitted from the periphery traveled quickly, the center, once alerted, would need too much information and too much time to generate

the specific precursors. In other words, the center would not be able to deliver an adequate number of the appropriate cells to the 'scene of the crime' quickly enough to avoid disaster. Therefore, to be most effective, these hypothetical regenerative centers would have to be scattered throughout the body. This is the same rationale for stationing firehouses throughout an entire city, to allow each unit to be able to more rapidly reach any fire location and efficiently intervene.

Our sophisticated regenerative system does not need to deploy totipotent cells into each organ. It would be enough to maintain in each organ sufficiently undifferentiated precursors with self-maintenance capabilities, as well as those necessary to replace the worn-out cells of the organ. Also desirable would be a physiological process that progresses relatively slowly to maintain tissue homeostasis but which could be converted, in the case of crisis, into a rapidly operating system. Consequently, this system would be highly effective at responding promptly to abruptly received, alarming feedback signals.

In the endocrine pancreas as well, long-lasting insulin-producing beta cells should be continuously, albeit quite slowly, replaced by newly generated cells. At the time of need, besides the possible replicative ability of the beta cells themselves (3), other regenerated cells should come from precursors, possibly located among pancreatic ductal cells (4). Thus, these regenerative units would be in close physical proximity to the endocrine tissue, the islets of Langerhans. When the pancreas is physically damaged, the pace of the physiologic reparative process accelerates and a more evident regeneration product can be observed.

This actually seems to be the message we receive from the recently published paper of Herrera's group (1) in which the inherent regenerative capacity of the adult pancreas to produce new beta cells was systematically studied. To generate a strong enough 'danger signal', an extreme situation was created in which near-total beta cell loss can be obtained at will to mimic type 1 diabetes pathology, but in the absence of autoimmunity. For this purpose, the authors used two *in vivo* genetic approaches: cell ablation combined with cell lineage tracing. Inducible, rapid cell removal (>99%) was obtained by administration of diphtheria toxin (DT) in transgenic mice in which the diphtheria toxin receptor (DTR) was expressed by the beta cells only. The systemic administration of DT permits an exquisite, specific ablation of almost all existing beta cells by apoptosis. Newly formed beta cells were easily monitored using a reliable cell lineage tracing. The results obtained surprisingly showed that the adult pancreas can actually generate new beta cells after their near-total loss, but mainly by reprogramming its glucagon-secreting alpha cells.

Taking all this information together, a physiologic scenario can be then envisaged in which tissue-specific precursors, present among pancreatic ductal cells (4), are generating alpha cells and beta cells (2). Beta cells, in turn, even if extremely slowly, replicate themselves to maintain homeostasis (3). However, once stimulated by a powerful danger signal, glucagon-positive alpha cells can then transdifferentiate into insulin-secreting beta cells to repair the damage (1).

In humans, without the help of lineage tracing, specific markers become necessary to recognize and eventually physically isolate tissue-specific precursors. However, even if these markers were already utilizable, intuitively one sees that isolating precursor cells from a patient's own pancreas would not be an easy task. Increasing their numbers *ex vivo* while avoiding the activation of differentiation pathways would also be problematic, as would facilitating their differentiation toward the wanted final product. Here again James Cameron anticipated a possible solution of the problem.

> *The T-1000, like an exceptional chameleon, blends into any scene, assuming the most appropriate appearance suggested by each environment it encounters. In the film, the T-1000 completely hides itself, becoming part of the black and white tiles of the floor of a hospital ward. It then regenerates from the linoleum into a human form. However, it does not resume its original human appearance; instead, it takes on the appearance of the security guard on duty where the patient, for whom it is looking, is unwillingly detained.*

Faithfully recreating the environment necessary to guide and facilitate a desired type of differentiation *in vitro* appears to be quite difficult. An easier solution might be to somehow isolate and then physically introduce a precursor into the already existing, appropriate environment like, e.g., the embryonic pancreas (5). The precursor would then be allowed to get 'acquainted' with its new surroundings by assuming the most appropriate appearance (i.e., phenotype) to better fit the new context. By becoming one with the new environment, the precursor may quickly convert into the product best equipped to repair the damage. The signals sent through host-secreted factors or by cell-to-cell contacts seem to be powerful enough to guide the differentiation process toward the most needed product, even across different lineage barriers. This ability to 'transdifferentiate' (i.e., generate a progeny belonging to a tissue lineage different from the one of origin) certainly is an astonishing discovery. A few years ago, no one would even speculate that a mammalian stem cell,

present in an adult individual, could still possess such an impressive plasticity. The possibility that new beta cells could be generated from 'adult' stem cells even passing through an alpha cell phenotype (1) offers a particularly appealing alternative, because it avoids the potential ethical problems associated with the use of embryonic stem cells.

However, even assuming the existence of these beta cell-specific precursors, we still do not know whether they are immortal or are actually subject to senescence, leaving us perhaps with a narrow window for intervention. This aspect may be especially relevant in diabetic individuals in whom the reparative process has been kept under check by autoimmune patrolling for a long period of time. In a case in which prompt intervention (e.g., immediately after the clinical onset of the disease) is not possible, would we still be able to repair the already 'seasoned', deleterious damage of the endocrine pancreas? In the absence of precursors, once they all might be already dead, which resources can still be used?

> The T-800 is abruptly catapulted into a foreign environment and another time period. Under the friendly guidance of a young boy, who patiently introduces human feelings, behaviors, and vernacular expressions into its newly accessible electronic memory, the T-800 assimilates this passively received and progressively accumulated information. Eventually it becomes able to interact in a more meaningful way with its surroundings. As a direct consequence, the T-800 starts experiencing human-like feelings and becomes so sensitive to human concerns that it decides on self-immolation as the only path that will halt or delay the destruction of the world it has begun to comprehend.

Many remarkable results have been obtained in the research laboratory by transfecting cells of a certain lineage (e.g., fibroblasts) with genes (i.e., *Oct4*, *Sox2*, *Klf4*) encoding different transcription factors able to convert these somatic cells into ones carrying the characteristics of pluripotent precursors. The human induced pluripotent stem (iPS) cells, in turn, could differentiate into cells of a different lineage, like insulin-producing cells, even if the quantity in which these precursors can be reliably generated seems to be quite limited (6). Furthermore, assuming that we could overcome these limiting aspects, the possibility of using human stem cell lines tailored *ad personam* is certainly revolutionary, even if it were quite inefficient, frequently unsuccessful, and consequently extremely expensive. This approach, while allowing us to bypass the big problem of allorejection, simultaneously opens the door to the possibility that these dividing cells will not stop growing once a specific, predetermined mass has been reached. In the situation in which these cells do not spontaneously stop proliferating, we could have, unknowingly and tragically, transplanted cancer precursors into our patients.

Finally, assuming that we would be able to establish pluripotent stem cell lines for each patient, and eventually derive from them a specific progeny with the correct phenotype, and that we could generate a sufficient number of the missing beta cells to satisfy the needs of the diabetic recipient, we would still have to solve the problem of recurrent autoimmunity. In patients with type 1 diabetes, autoimmunity not only damages the original endocrine tissue, bringing them to the clinical onset of the disease, but also efficiently limits its reparative process. In fact, autoreactive, diabetogenic T-cell clones, escaped from thymic control (7), seem to be able to systematically kill newly generated beta cells with which the precursors try to replace the ones that are lost. Once transplanted into diabetic mice or humans, syngeneic, healthy beta cells are quickly killed by these same perpetrators, namely $CD8^+$ effector T-cells (8).

This autoimmune process is successfully annihilated in the diabetes-prone [e.g., the non-obese diabetic (NOD)] mouse either by substituting all or a part of the immunocompetent cell pool of the recipient with bone marrow cells from a diabetic-resistant donor. Complete substitution is accomplished with conventional bone marrow transplant techniques, and partial substitution by establishing hematopoietic chimerism (9, 10). If these processes were to proceed in humans, they should be sufficient to ensure the recipient's well-being long enough to let him or her benefit from the positive consequences of the laborious, regenerative process. However, more important is the consideration that the successful engraftment of the transplanted bone marrow, or the establishment of a steady hematopoietic chimerism, would have to be obtained and eventually maintained without the use of immunosuppressive agents. This is because these potent drugs, by definition, would kill not only the immunocompetent cells of the recipient but also the beta cells themselves, which are particularly sensitive to the toxicity of the immunosuppressive agents (11). This would, of course, completely defeat the purpose of the transplant.

Perhaps more easy to implement is another approach successfully used in the mouse to stop autoimmunity. Dendritic cells (DCs) are the body's sentinels largely responsible for host surveillance against microenvironmental anomalies including pathogen invasion, infection, and damaged tissue architecture. In a functionally immature state (characterized by low to absent expression of costimulatory molecules such as

CD40, CD80, and CD86), DCs are powerful agents of immune hyporesponsiveness. Exogenous administration of functionally immature DCs achieves long-term and stable allograft survival in a variety of mouse and rat models and prevents a number of autoimmune diseases. Mechanistically, functionally immature DCs act by inducing anergy of the dangerous effector T-cells, either via direct cell contact and/or cytokines and by upregulating the number and function of regulatory T-cell subsets. It has also been shown that *in vitro* administration of nuclear factor-kappa B (NF-kappa B) decoys to DC as well as direct targeting of CD40, CD80, and CD86 with antisense oligodeoxyribonucleotides (AS-ODNs), reduce costimulatory molecule expression levels, producing functionally immature DCs capable of preventing or even reversing new-onset diabetes, once reintroduced into the diabetic recipient, the same NOD mouse from which they were originally collected (12). If we would be able to somehow stop autoimmunity, then it would be sufficient to characterize the factors able to trigger the regenerative process of the beta cell, allowing us to bypass quantitative and chronological limits of resident precursor cells and to reconstitute in this way an efficient glycemic control in our young patients (13).

Diabetic patients must check their blood glucose levels and be injected with insulin at least four times a day. Concurrently, they live with the constant threat of unpredictable incidents of hypoglycemia and the persistent worry of future damage associated with the disease state. Therefore, these patients are probably not enthusiastic about the prospect of waiting for the day in the distant future when the resolution of all the problems of the extremely interesting, yet extremely complex process of tissue regeneration are resolved, before they can have a cure. They would likely look forward to a cure sooner, rather than later. However, it is only in the movies where optimism always prevails against all odds. In science, optimism is generally tempered by the concerns and critiques of peers, which serve to raise questions and may actually rectify errors. Despite some scientific skepticism, the prospect of gene therapy-based treatments remains intriguing and the use of human stem cell research carries with it enormous scientific potential in the treatment and possible cure of many diseases. As we wait, then, for a successful and perhaps not too distant clinical application of the regenerative capabilities of our endocrine pancreas, we may have to be hopeful and just satisfied by the obtained evidence that supports the rights for the beta cell to proudly repeat the statement made famous by the T-800:

'I'll be back!'.

References

1. THOREL F, NÉPOTE V, AVRIL I et al. Conversion of adult pancreatic alpha cells to beta cells after extreme beta cells loss. Nature 2010: 464: 1149–1154.
2. TRUCCO M. Regeneration of the pancreatic beta cell. J Clin Invest 2005: 115: 5–12.
3. DOR Y, BROWN J, MARTINEZ OI, MELTON DA. Adult pancreatic beta cells are formed by self-duplication rather than stem-cell differentiation. Nature 2004: 429: 41–46.
4. JUHL K, BONNER-WEIR S, SHARMA A. Regenerating pancreatic beta cells: plasticity of adult pancreatic cells and the feasibility of in-vivo neogenesis. Curr Opin Organ Transplant 2010: 15: 79–85.
5. XU X, D'HOKER J, STANGÉ G et al. Beta cells can be generated from endogenous progenitors in injured adult mouse pancreas. Cell 2008: 132: 197–207.
6. MAEHR R, CHEN S, SNITOW M et al. Generation of pluripotent stem cells from patients with type 1 diabetes. PNAS 2009: 106: 15768–15773.
7. FAN Y, RUDERT WA, GRUPILLO M, HE J, SISINO G, TRUCCO M. Thymus-specific deletion of insulin induces autoimmune diabetes. EMBO J 2009: 28: 2812–2824.
8. SUTHERLAND DE, SIBLEY R, XU XZ et al. Twin-to-twin pancreas transplantation: reversal and reenactment of the pathogenesis of type 1 diabetes. Trans Assoc Am Physicians 1984: 97: 80–87.
9. HUANG Y, KUCIA M, HUSSAIN LR et al. Bone marrow transplantation temporarily improves pancreatic function in streptozotocin-induced diabetes: potential involvement of very small embryonic-like cells. Transplantation 2010: 89: 677–685.
10. NIKOLIC B, ONOE T, TAKEUCHI Y et al. Distinct requirements for achievement of allotolerance versus reversal of autoimmunity via nonmyeloablative mixed chimerism induction in NOD mice. Transplantation 2010: 15: 23–32.
11. NIR T, MELTON DA, DOR Y. Recovery from diabetes in mice by beta cell regeneration. J Clin Invest 2007: 117: 2553–2561.
12. MACHEN J, HARNAHA J, LAKOMY R, STYCHE A, TRUCCO M, GIANNOUKAKIS N. Antisense oligonucleotides down-regulating costimulation confer diabetes-preventive properties to nonobese diabetic mouse dendritic cells. J Immunol 2004: 173: 4331–4341.
13. PHILLIPS B, GIANNOUKAKIS N, TRUCCO M. Dendritic cell-based therapy in type 1 diabetes mellitus. Expert Rev Clin Immunol 2009: 5: 325–339.

Distinct growth hormone receptor signaling modes regulate skeletal muscle development and insulin sensitivity in mice

Mahendra D. Mavalli,[1] Douglas J. DiGirolamo,[1] Yong Fan,[2] Ryan C. Riddle,[1] Kenneth S. Campbell,[3] Thomas van Groen,[4] Stuart J. Frank,[4,5,6] Mark A. Sperling,[2] Karyn A. Esser,[3] Marcas M. Bamman,[7] and Thomas L. Clemens[1,8]

[1]Department of Orthopaedic Surgery, Johns Hopkins University School of Medicine, Baltimore, Maryland, USA.
[2]Department of Pediatrics, University of Pittsburgh School of Medicine, Pittsburgh, Pennsylvania, USA. [3]Center for Muscle Biology, University of Kentucky College of Medicine, Lexington, Kentucky, USA. [4]Department of Cell Biology and [5]Department of Medicine, Division of Endocrinology, Diabetes and Metabolism, University of Alabama at Birmingham, Birmingham, Alabama, USA. [6]Endocrinology Section, Medical Service, Veterans Affairs Medical Center, Birmingham, Alabama, USA. [7]Department of Physiology and Biophysics, University of Alabama at Birmingham, Birmingham, Alabama, USA. [8]Veterans Administration Medical Center, Baltimore, Maryland, USA.

Skeletal muscle development, nutrient uptake, and nutrient utilization is largely coordinated by growth hormone (GH) and its downstream effectors, in particular, IGF-1. However, it is not clear which effects of GH on skeletal muscle are direct and which are secondary to GH-induced IGF-1 expression. Thus, we generated mice lacking either GH receptor (GHR) or IGF-1 receptor (IGF-1R) specifically in skeletal muscle. Both exhibited impaired skeletal muscle development characterized by reductions in myofiber number and area as well as accompanying deficiencies in functional performance. Defective skeletal muscle development, in both GHR and IGF-1R mutants, was attributable to diminished myoblast fusion and associated with compromised nuclear factor of activated T cells import and activity. Strikingly, mice lacking GHR developed metabolic features that were not observed in the IGF-1R mutants, including marked peripheral adiposity, insulin resistance, and glucose intolerance. Insulin resistance in GHR-deficient myotubes derived from reduced IR protein abundance and increased inhibitory phosphorylation of IRS-1 on Ser 1101. These results identify distinct signaling pathways through which GHR regulates skeletal muscle development and modulates nutrient metabolism.

Introduction

Mammalian skeletal muscle has evolved to perform a diverse set of functions, including locomotion, breathing, protecting internal organs, and coordinating global energy expenditure. Skeletal muscle is formed and regenerated through a highly regulated process characterized by myoblast differentiation and fusion into multinucleated syncytia. During embryonic development, specification of mesodermal precursor cells into the myogenic lineage is controlled by signals from surrounding tissues and requires upregulation of several factors, including paired-box transcription factor 7 (pax-7) and basic helix-loop-helix transcriptional activators of the myogenic regulatory factor family, MyoD and Myf-5 (1). The proliferating precursor cells/myoblasts withdraw from the cell cycle and initiate muscle-specific gene expression (2, 3). Myoblasts then initially fuse to form nascent myotubes, with relatively few nuclei, through a highly ordered set of cellular events, including recognition, adhesion, alignment, and membrane union. Subsequent recruitment and fusion of additional myoblasts gives rise to multinucleated myotubes that ultimately mature to give rise to skeletal muscle fibers. The fusion process is controlled, in part, by the actions of calcium-sensitive transcription factors of the nuclear factor of activated T cells (NFAT) family (4, 5). During myoblast fusion,

the nuclear translocation of NFATc2 transcriptionally activates IL-4, a cytokine essential for myoblast recruitment (6).

The growth hormone/IGF-1 (GH/IGF-1) axis represents an important physiological regulatory mechanism for coordinating postnatal skeletal muscle expansion and hypertrophy. Administration of GH to both animals and GH-deficient humans improves muscle strength and reduces body fat (7–9). Moreover, recent studies have shown that mice globally deficient in GH receptor (GHR) have reduced muscle mass with defective myofiber specification and growth (10). Such studies clearly demonstrate the importance of GH in skeletal muscle development but do not address the mechanisms responsible for these effects.

GH exerts growth-promoting and metabolic effects in target tissues (11) by binding to the transmembrane GHR and triggering enhanced GHR association with, and activation of, the cytoplasmic tyrosine kinase JAK2 (12, 13). Three major signaling systems activated in response to GH include STATs (most notably STAT5b), phosphoinositide 3-kinase (PI3K), and Erk (14, 15). STAT5b activation by GH results in transcriptional activation of GH target genes, including IGF-1 (16, 17). Many but not all of the anabolic effects of GH are exerted indirectly via this stimulation of IGF-1 from liver and peripheral tissues (18–27).

IGF-1 is a small polypeptide with homology to proinsulin, which is produced by many cell types. IGF-1 signals via the type-1 IGF-1 receptor (IGF-1R), a widely expressed cell surface heterotetramer, highly similar to the IR, which possesses intrinsic kinase activity in its cytoplasmic domains (28, 29). Activated IGF-1R engages the Erk and PI3K pathways via phosphorylation of SHC

and IRS-1 to induce proliferation, inhibit apoptosis, and elicit a number of other cellular responses (30, 31). The availability of either systemic or locally produced IGF-1 to its cognate receptor is determined by a multicomponent delivery system composed of a family of IGF-binding proteins (32–34), which serve to prevent or facilitate access to IGF-1R.

In this study, we sought to define the mechanisms of GH action in skeletal muscle and specifically attempted to distinguish direct mechanisms of GH action from those mediated indirectly by IGF-1. To accomplish this, we created genetic mouse models with targeted disruption of GHR or IGF-1R, specifically in skeletal muscle. Our studies using these mice show that GH mediates skeletal muscle development by enhancing myoblast fusion in an IGF-1–dependent manner. By contrast, disruption of the GHR in skeletal muscle produces marked alterations in muscle nutrient uptake and insulin sensitivity in an IGF-1–independent manner.

Results

GH-induced myoblast proliferation and fusion is mediated by IGF-1. The anabolic effects of GH in skeletal muscle are well documented (7–9), but despite some evidence to suggest that these effects might be mediated by IGF-1 (35), the precise mode of GH action in skeletal muscle remains unclear. To begin to define the mechanism of GH action in skeletal muscle in vitro, we examined the effect of GH on IGF-1 production, myoblast proliferation, and myoblast fusion, using a primary myoblast culture system that has been described previously (36) (Supplemental Figure 1, A–F; supplemental material available online with this article; doi:10.1172/JCI42447DS1). Treatment of primary myoblasts with GH acutely increased *Igf1* mRNA by 3 hours, with maximal mRNA levels achieved by 6 hours (Figure 1A). Further, acute exposure of myoblasts to GH did not affect proliferation, as indexed by BrdU incorporation at 8 hours (prior to GH-induced IGF-1 protein production), whereas exogenous IGF-1 significantly increased primary myoblast proliferation (Figure 1B). These results are compatible with a mechanism in which GH induces myoblast production of IGF-1, and this IGF-1, in turn, stimulates myoblast proliferation through an autocrine mechanism.

We next examined the effect of GH on myoblast fusion. In this in vitro system, myoblasts fuse to form multinucleated myotubes in 2 stages. In the first phase (24 hours after induction of differentiation), 2 myoblasts fuse to form a nascent myotube. During the next phase (hours 24–48), additional myoblasts fuse to this nascent myotube to increase the number of nuclei, ultimately producing a larger, fully differentiated myotube. Myoblasts exposed to GH during the first 24-hour period (nascent myotube formation) fused similarly to controls, as assessed by the number of nuclei per myotube (Figure 1C). By contrast, cultures treated with GH for the entire 48-hour period of differentiation, or alternatively only during hours 24–48 (myonuclei accumulation), had significantly higher nuclei/myotube ratios (Figure 1C). This result suggests that GH affects myofiber development by stimulating accumulation of additional myonuclei into nascent myotubes.

We next sought to determine the requirement of GHR for basal myoblast fusion. Primary myoblasts isolated from mice carrying homozygous floxed *Ghr* alleles were infected with adenoviruses expressing either Cre-recombinase (adenoCre) to selectively excise the GHR (Supplemental Figure 1G) or adenoGFP as a control. Disruption of GHR did not alter basal myoblast fusion (Figure 1D), suggesting that GHR is not essential for basal levels of fusion, at least under these experimental conditions in vitro. As expected,

disruption of GHR abolished GH-stimulated fusion observed in control myoblasts (Figure 1D). Addition of IGF-1 to myoblasts significantly increased the number of nuclei per myotube, regardless of GHR status (Figure 1D). Moreover, primary myoblasts lacking the IGF-1R, generated in a similar fashion as those above (Supplemental Figure 1H), failed to fuse in response to GH (Figure 1E). To ensure that deletion of IGF-1R did not introduce a critical defect, such that myoblasts would be unable to respond to any fusion stimulus, control and ΔIGF-1R myoblasts were also treated with IL-4, which is known to increase myoblast fusion (4). IL-4 did not significantly increase the number of nuclei per myotube in ΔIGF-1R myoblasts (Supplemental Figure 1I). However, IL-4 increased the percentage of fused myoblasts (fusion index), regardless of IGF-1R status (Supplemental Figure 1J). By contrast, GH had no effect on the number of nuclei per myotube or the fusion index in ΔIGF-1R myoblasts (Supplemental Figure 1, I and J). Taken together, these results suggest that the anabolic effect of GH to increase myoblast fusion is mediated by IGF-1. Further, IGF-1R appears to be critical for the accrual of myonuclei into nascent myotubes, at least in the context of our in vitro model.

GH induces myoblast fusion via NFATc2-induced IL-4 production. As described above, previous studies have implicated the NFAT family of transcription factors as critical mediators of myoblast fusion (4, 5). To investigate the potential involvement of the NFAT/IL-4 pathway in GH-induced myoblast fusion, we determined the effects of GH and IGF-1 on NFAT abundance and nuclear import. Initial studies indicated that NFATc2 was abundantly expressed by primary mouse myoblasts, whereas other NFAT isoforms were either absent or expressed at low levels (data not shown). Treatment of primary myoblasts with GH or IGF-1 for 1 hour induced NFATc2 nuclear localization (Figure 1F). Moreover, myoblasts carrying an NFAT luciferase reporter that were treated with either GH or IGF-1 significantly increased reporter activity over that observed in untreated cells (Figure 1G). Additionally, GH increased *Il4* mRNA expression in primary myoblasts (Figure 1H), in accordance with previous studies (6). These findings suggest that GH and/or IGF-1 intersect with the NFATc2/IL-4 pathway to promote primary myoblast fusion.

GHR is required for normal myofiber specification, myonuclei accumulation, and muscle function. To examine the role of individual components of the GH/IGF-1 axis in skeletal muscle development in vivo, we created 2 mouse models that lacked either GHR or IGF-1R in skeletal muscle. Details about the generation of these animals are illustrated in Supplemental Figure 2 and described in the Methods. Mice lacking GHR (ΔGHR mice) were born at the expected Mendelian frequency and were viable. Deletion of *Ghr* mRNA from skeletal muscle was confirmed by real-time PCR (Figure 2A), and importantly, removal of the GHR from skeletal muscle did not affect *Igf1r* mRNA expression levels (Figure 2B). Expression of *Igf1* mRNA in skeletal muscle was increased at 6 weeks (Figure 2C), possibly a result of compensation by other pathways known to activate IGF-1 production in skeletal muscle, most likely androgens (37, 38). However, *Igf1* mRNA in ΔGHR mutants declined to levels below those observed in control animals by 16 weeks (Figure 2C). Serum levels of GH and IGF-1 in ΔGHR mice, also measured at 16 weeks of age, were not different from control mice (data not shown). Quantitative histomorphometric analysis of the medial gastrocnemius muscle from ΔGHR and control littermates was performed at 6 and 16 weeks (Figure 2, D–G). At 6 weeks, the number of myonuclei per 100 myofibers in cross-section was
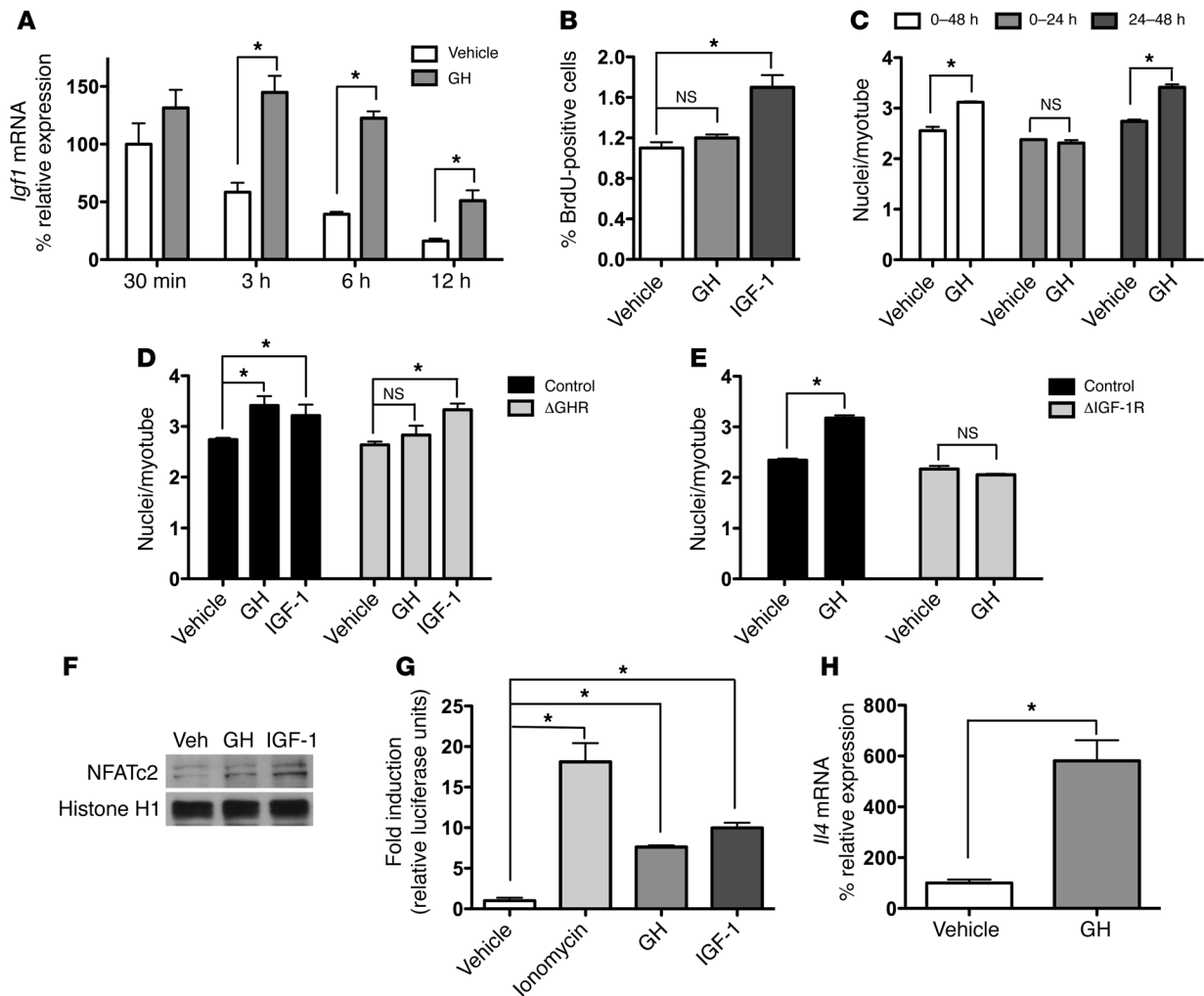
Figure 1
GH-induced myoblast proliferation and fusion are mediated by IGF-1 production and intersect the NFATc2/IL-4 pathway. (**A**) Primary mouse myoblasts were serum starved for 10 hours before stimulation with GH. Real-time PCR was performed using primers for IGF-1 at indicated times. (**B**) Myoblasts were serum starved for 10 hours before stimulation with GH or IGF-1 for 8 hours, with BrdU exposure for the full 8 hours of treatment. The percentage of BrdU-positive cells was assessed by flow cytometry. (**C**) Myoblasts were induced to differentiate and treated with GH for 0–48 hours, 0–24 hours, or 24–48 hours of differentiation. (**D**) GHR-floxed myoblasts were infected with adenoGFP (control) or adenoCre (ΔGHR) and differentiated in the presence of vehicle, GH, or IGF-1 for 48 hours. (**E**) IGF-1R–floxed myoblasts were infected with adenoGFP (control) or adenoCre (ΔIGF-1R) as treated in **D**. (**F**) Wild-type myoblasts were serum starved for 10 hours before stimulation with vehicle (Veh), GH, or IGF-1 for 1 hour and harvest of nuclear protein extracts. (**G**) Myoblasts were transfected with an NFAT luciferase reporter construct before induction of differentiation for 24 hours and treatment with vehicle, ionomycin, GH, or IGF-1 for 5 hours. (**H**) Myoblasts were serum starved for 10 hours before treatment with vehicle or GH for 5 hours. Real-time PCR was performed using primers for IL-4. All data shown is representative of at least 3 separate experiments performed from separate muscle cell preparations. Error bars indicate SEM. *P < 0.05.

lower in ΔGHR mice compared with that of control littermates for both fiber types at both time points (Figure 2, H and K). The proportion of type I fibers was lower in the ΔGHR gastrocnemius compared with that of controls (Figure 2I), whereas the proportion of type II fibers were concomitantly higher than that of type I fibers (Figure 2I). At 6 weeks, type I and type II myofiber sizes did not differ between ΔGHR and control mice (Figure 2J). However, ΔGHR mice failed to attain myofiber diameters comparable with those of controls for both type I and type II fibers by 16 weeks of age (Figure 2M). These changes in muscle physiology persisted through 26 weeks of age (Supplemental Figure 3). The reduced number of myonuclei and smaller myofibers in ΔGHR mice are

consistent with deficient myoblast fusion demonstrated in vitro. Taken together, these results document the requirement of GHR for proper skeletal muscle development in vivo.

We next assessed the functional consequences of GHR disruption in skeletal muscle. Groups of 26-week-old control and ΔGHR mice were subjected to the standard grip strength and rotarod tests. Mice were analyzed at 26 weeks of age, because, at this time, body weight reached a plateau in both ΔGHR and control mice (see below), and therefore, any developmental changes resulting from GHR deletion in skeletal muscle would be expected to have reached a steady state. At this time point, grip strength was lower (Figure 2N) and measures of rotarod endurance performance
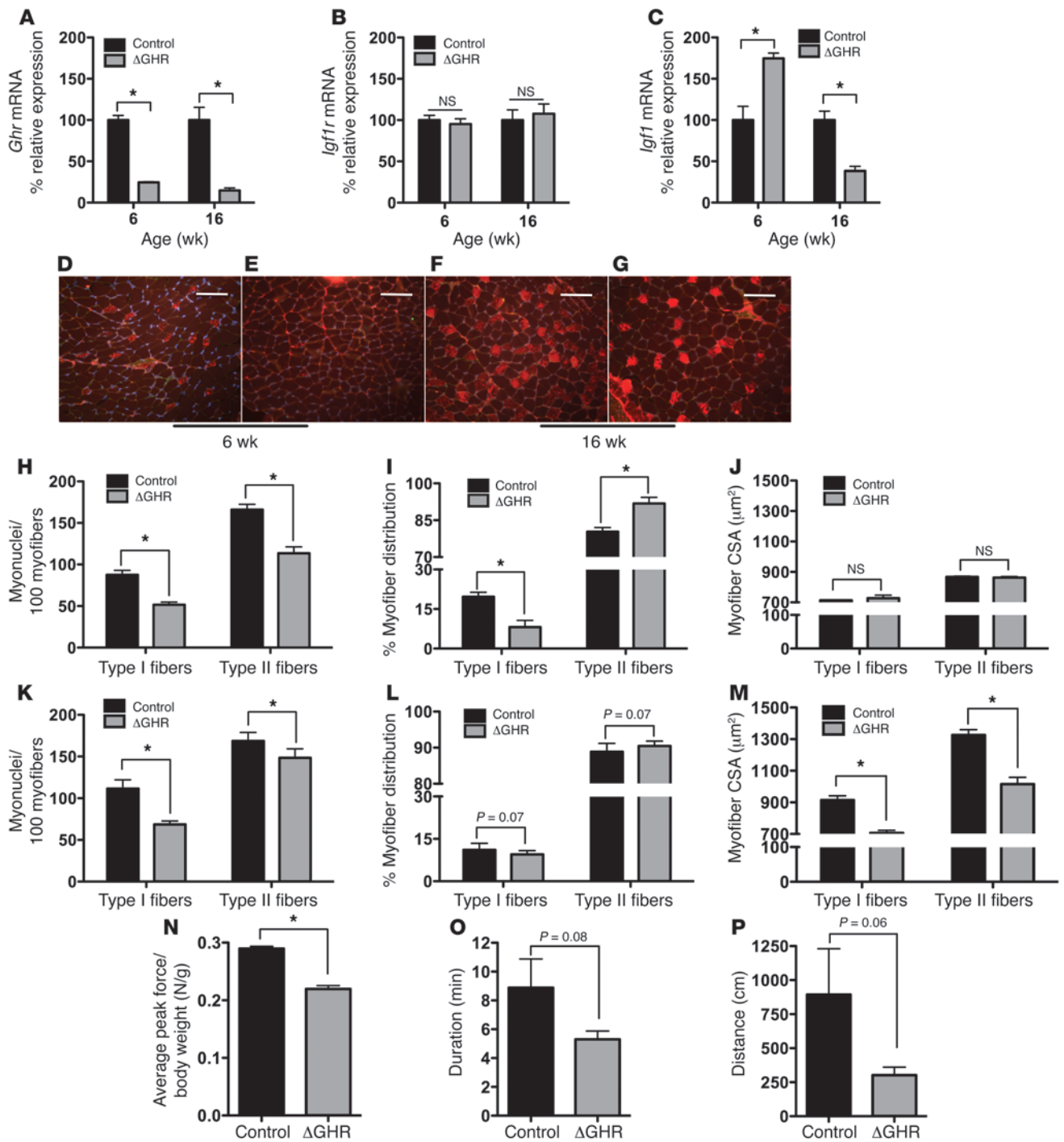
Figure 2
GHR is required for normal myofiber specification, myonuclei accumulation, and muscle function. mRNA was harvested from the gastrocnemius muscles of control and ΔGHR mice, and real-time PCR was performed using primers for (**A**) *Ghr*, (**B**) *Igf1r*, and (**C**) *Igf1*. (**D–G**) Sections of medial gastrocnemius from control and ΔGHR mice were visualized using antibodies directed against MHC type I and laminin and counterstained with Hoechst 33258 to visualize myonuclei. Scale bars: 80 μm. (**H–M**) Histomorphometric analyses of myonuclei per 100 myofibers, percentage myofiber distribution, and myofiber diameter (CSA) were performed on sections described above for (**H–J**) 6-week-old and (**K–M**) 16-week-old control and ΔGHR mice. Muscle performance in 26-week-old control and ΔGHR mice was assessed by (**N**) grip strength and (**O** and **P**) rotarod testing, as described in Methods. For all studies shown, *n* = 6 for control and ΔGHR at all time points. Error bars indicate SEM. *$P < 0.05$.
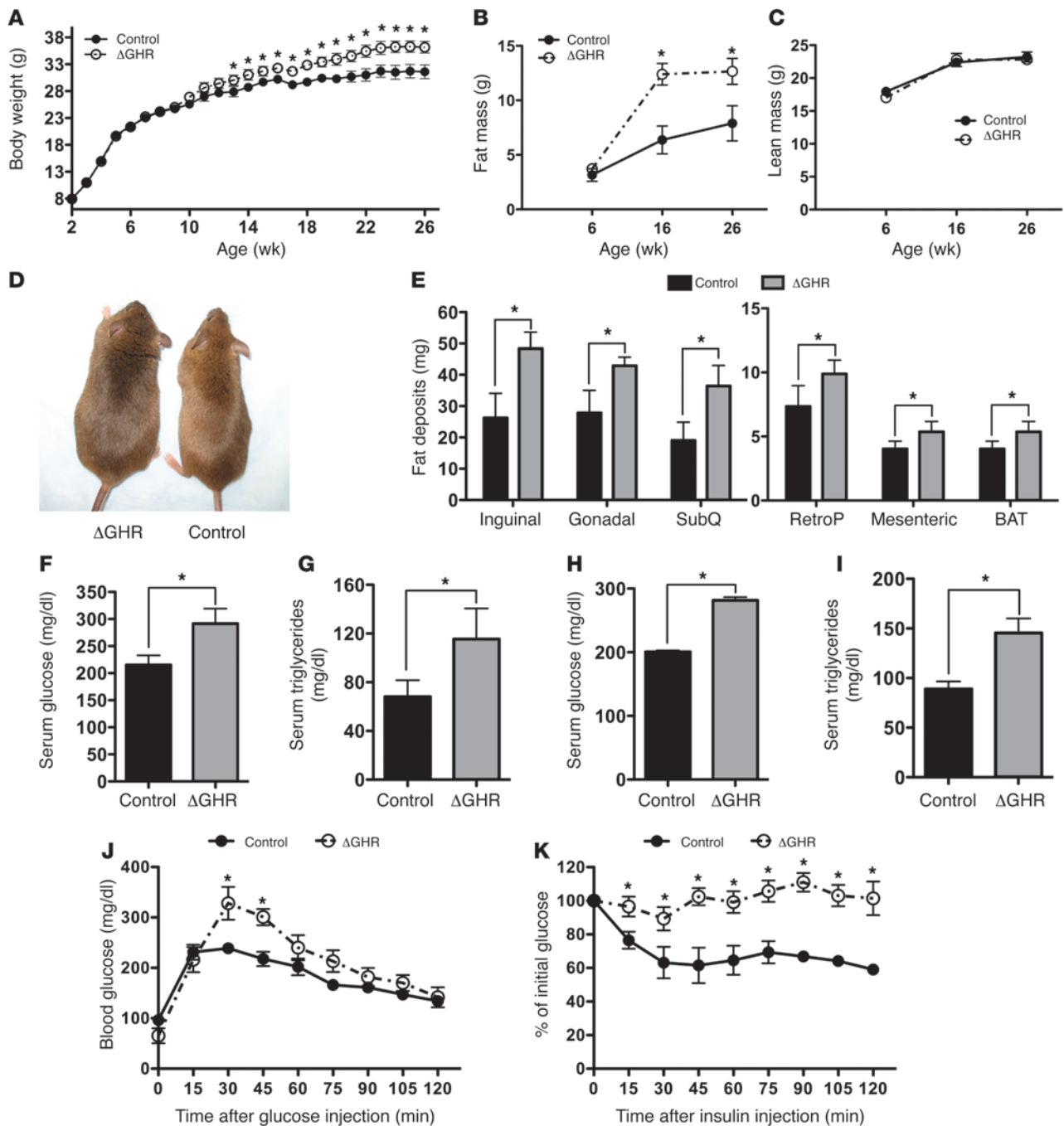
Figure 3
Loss of GHR in skeletal muscle causes peripheral adiposity, glucose intolerance, and insulin resistance. (**A**) Control ($n = 9$) and ΔGHR ($n = 11$) mice were weighed weekly from 2 to 26 weeks of age (image in **D** was taken at 26 weeks). qMR analysis of (**B**) fat and (**C**) lean mass in control and ΔGHR mice at 6, 16, and 26 weeks of age. (**E**) Fat pad mass at 26 weeks. SubQ, subcutaneous; RetroP, retroperitoneal; BAT, brown adipose tissue. (**F–I**) Ad libitum serum glucose and triglyceride concentration at (**F** and **G**) 16 weeks and (**H** and **I**) 26 weeks of age. Control and ΔGHR mice were also subjected to (**J**) GTTs and (**K**) ITTs, as described in Methods. Unless otherwise indicated, $n = 6$ for control and ΔGHR at all time points. Error bars indicate SEM. *$P < 0.05$.

tended to be lower (Figure 2, O and P) in ΔGHR mice compared with controls. These results suggest that the disruption of GHR in skeletal muscle and the consequent histomorphometric changes in myofiber type and size and myonuclei number result in functionally impaired skeletal muscle.

Loss of GHR in skeletal muscle causes peripheral adiposity, glucose intolerance, and insulin resistance. Sequential measurement of the body weights of ΔGHR mice showed an unanticipated increase in body weight of ΔGHR mutant mice relative to that of their control littermates (Figure 3, A and D) that first became apparent
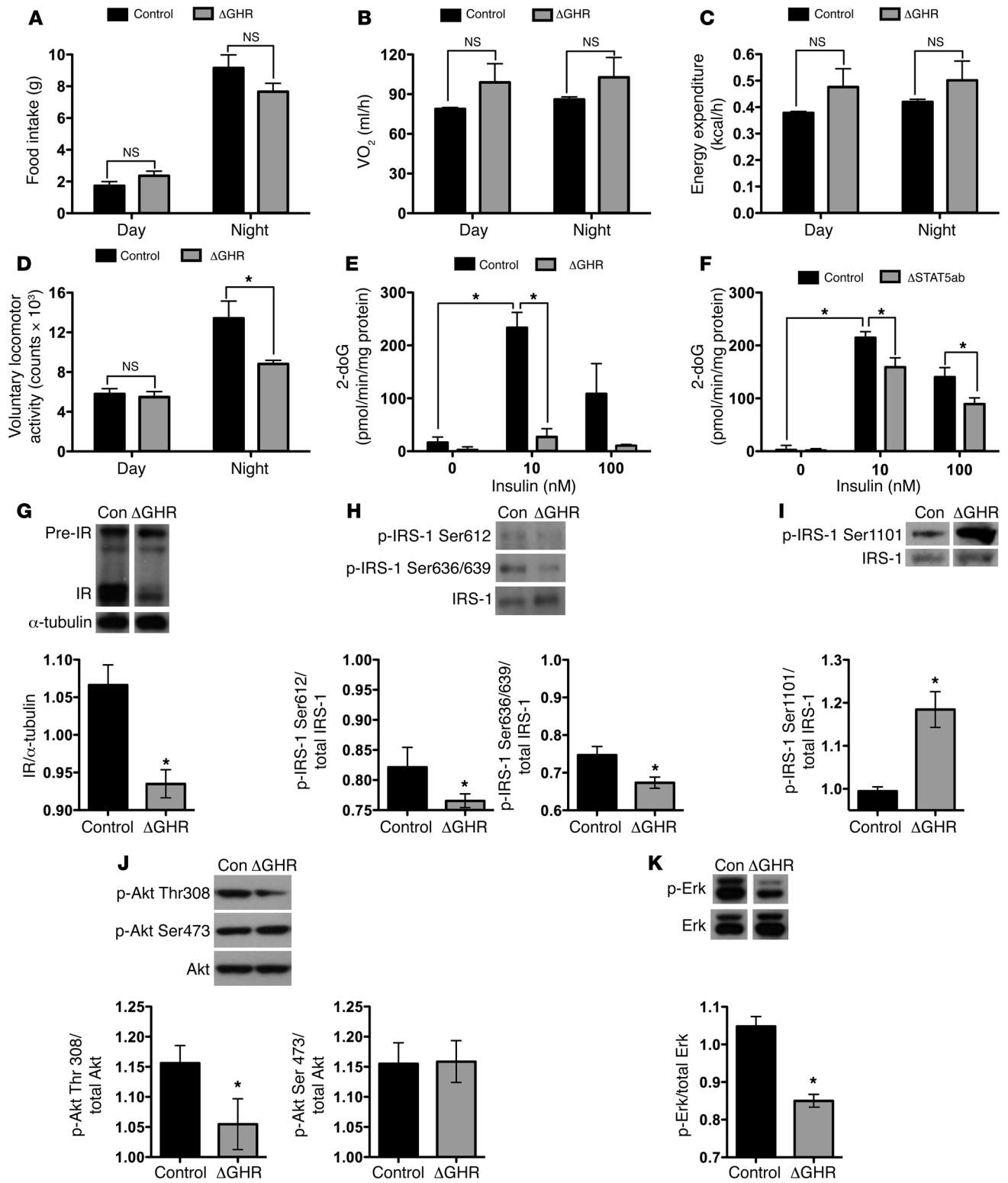
Figure 4

Metabolic phenotype of ΔGHR mice is associated with skeletal muscle insulin resistance. (**A**) Food intake of 26-week-old control and ΔGHR mice. (**B**) Oxygen consumption (VO₂) and (**C**) energy expenditure, as assessed by indirect calorimetry. (**D**) Voluntary locomotor activity assessed by computer-monitored infrared beam breaks (*n* = 4 control and ΔGHR mice for **A**–**D**). (**E** and **F**) Myoblasts carrying (**E**) floxed GHR alleles or (**F**) floxed STAT5ab alleles were infected with adenoGFP (control) or adenoCre (ΔGHR or ΔSTAT5ab, respectively). Myoblasts were then serum starved for 12 hours, before a 1-hour pretreatment with vehicle or insulin, and then pulsed with 2-doG. Radiolabeled glucose uptake was determined by liquid scintillation counting. (**G**–**K**) Protein lysates were harvested from differentiated control and ΔGHR primary myotubes and subjected to SDS-PAGE analysis. Membranes were immunoblotted with antibodies directed against the proteins indicated. Membranes were stripped and reprobed for the indicated loading control protein. In some cases, additional irrelevant lanes between those shown were removed (indicated by separating white space). Bands for the indicated proteins were quantified based on gray density, as described in the Methods, and normalized against respective loading control proteins. All in vitro data shown is representative of at least 3 separate experiments performed from separate muscle cell preparations. Error bars indicate SEM. *$P < 0.05$.

at 12 weeks. Quantitative magnetic resonance (qMR) showed that ΔGHR mice had increased fat mass (Figure 3B), compared with control littermates, with no significant differences in lean mass (Figure 3C). Fat pad mass was higher at all sites in ΔGHR mice relative to that of controls (Figure 3E).

The peripheral adiposity observed in ΔGHR mice suggested disturbances in nutrient metabolism brought about by loss of GH action in skeletal muscle. Consistent with this idea, ΔGHR mice had elevated serum glucose (Figure 3, F and H) and triglyceride levels (Figure 3, G and I) in the fed state, although no differences were observed in serum insulin concentration (data not shown). These biochemical features, together with the changes in body composition in the ΔGHR mice, indicated the development of insulin resistance. We therefore performed standard glucose tolerance tests (GTTs) and insulin tolerance tests (ITTs). Fasting baseline glucose concentrations were similar in ΔGHR and control mice, but glucose excursions in ΔGHR mice were significantly higher compared with those of controls (Figure 3J). Likewise, reductions in plasma glucose levels after i.p. injection of insulin were less pronounced in ΔGHR mice (Figure 3K), consistent with the development of insulin resistance. Food intake (Figure 4A) and metabolic rate, as assessed by indirect calorimetry (Figure 4, B and C), were not significantly affected in ΔGHR mice, whereas nighttime voluntary locomotor activity was lower compared with that of control animals (Figure 4D).

To examine the molecular mechanisms responsible for the development of insulin resistance in ΔGHR mice, we compared insulin-stimulated 2-deoxy-[³H] glucose (2-doG) uptake in control and ΔGHR myoblasts. Cre-mediated disruption of GHR from myoblasts resulted in a dramatic reduction (~90%) of insulin-stimulated glucose uptake compared with that of control myoblasts (Figure 4E). Since activation of STAT5b by GH induces transcription of a number of GH target genes, including those involved in glucose and triglyceride uptake and metabolism in skeletal muscle, we assessed insulin-stimulated glucose uptake in myoblasts lacking STAT5 (ΔSTAT5ab). Uptake of 2-doG was reduced by 30% in ΔSTAT5ab myoblasts compared with controls (Figure 4F). The

comparatively modest decrease (30% vs. 90%) suggested that GH regulates insulin responsiveness through additional mechanisms. To investigate further the mechanism for loss of insulin responsiveness in ΔGHR cells, we directly examined insulin signaling components in control and ΔGHR myotubes. Immunoblotting of whole cell lysates from ΔGHR myotubes revealed a significant reduction in IR abundance compared with that of control myotubes (Figure 4G). We next examined 3 sites on IRS-1, which are known to be inhibitory to insulin signaling when phosphorylated. Basal phosphorylation of Ser 612 and Ser 636/639 was significantly decreased in ΔGHR myotubes (Figure 4H), whereas phosphorylation of IRS-1 on Ser 1101 (39) was markedly increased in ΔGHR myotubes (Figure 4I). Measurement of signaling effectors downstream of IRS-1 showed that basal phosphorylation of the receptor-activated, PI-3K–mediated Akt activation loop (Thr 308) was significantly decreased in ΔGHR myotubes compared with controls (Figure 4J), consistent with the downregulation of IR. In addition, basal phosphorylation of Ser 473 on Akt, which can be activated by a number of signaling pathways, was unchanged in ΔGHR myoblasts (Figure 4J). Finally, basal Erk phosphorylation was also significantly decreased in ΔGHR myotubes compared with that of controls (Figure 4K). These results suggest that loss of GHR in skeletal muscle disrupts nutrient metabolism by desensitizing skeletal muscle to insulin action at multiple points in the IR signaling pathway.

Mice lacking IGF-1R in skeletal muscle phenocopy the skeletal muscle defects, but not the metabolic abnormalities, of ΔGHR mutants. The in vitro studies described above suggested that the effects of GH on myoblast fusion and development were largely (if not exclusively) mediated by IGF-1. To test the importance of IGF-1 signaling for skeletal muscle development in vivo, we created an additional mouse model in which the IGF-1 receptor (ΔIGF-1R mice) was selectively disrupted in skeletal muscle (Supplemental Figure 2). Mice lacking the IGF-1R exhibited marked alterations in skeletal muscle development. *Igf1r* mRNA expression was reduced by more than 90% in the gastrocnemius muscle of ΔIGF-1R mice (Figure 5A), with no change in *Ghr* mRNA expression (Figure 5B). By contrast, *Igf1* mRNA expression (Figure 5C) and *Igf2* mRNA expression (data not shown) increased at 16 weeks. While we do not fully understand the reason for elevated *Igf1* mRNA in these mice, it is possible that compensatory pathways, such as androgens (37, 38), or loss of feedback inhibition of IGF-1 via autocrine effects through its receptor (40), led to increased IGF-1 production. Histomorphometric analysis of the medial gastrocnemius from 6- and 16-week-old control and ΔIGF-1R mice (Figure 5, D–G) revealed lower myonuclei numbers (Figure 5, H and K) and smaller myofibers in both type I and type II fibers in ΔIGF-1R mice (Figure 5, J and M). Similar to that of ΔGHR mice, type I fibers appeared to be preferentially lost (Figure 5, I and L), although the perturbation of fiber type distribution persisted throughout all examined time points in ΔIGF-1R mice.

Unlike the ΔGHR mice, which gained weight postnatally, mice lacking IGF-1R in skeletal muscle failed to attain normal body weight as they aged (Figure 5N). Analysis of body composition by qMR indicated ΔIGF-1R mice had less fat mass at 16 weeks (Figure 5O), with no change in serum glucose (Figure 5Q), triglyceride (Figure 5R), or insulin levels (data not shown). In addition, ΔIGF-1R mice failed to achieve normal lean mass by 16 weeks (Figure 5P), likely due to lesser muscle mass. In support of this notion, dual-energy X-ray absorptiometry (DXA) analysis also showed a
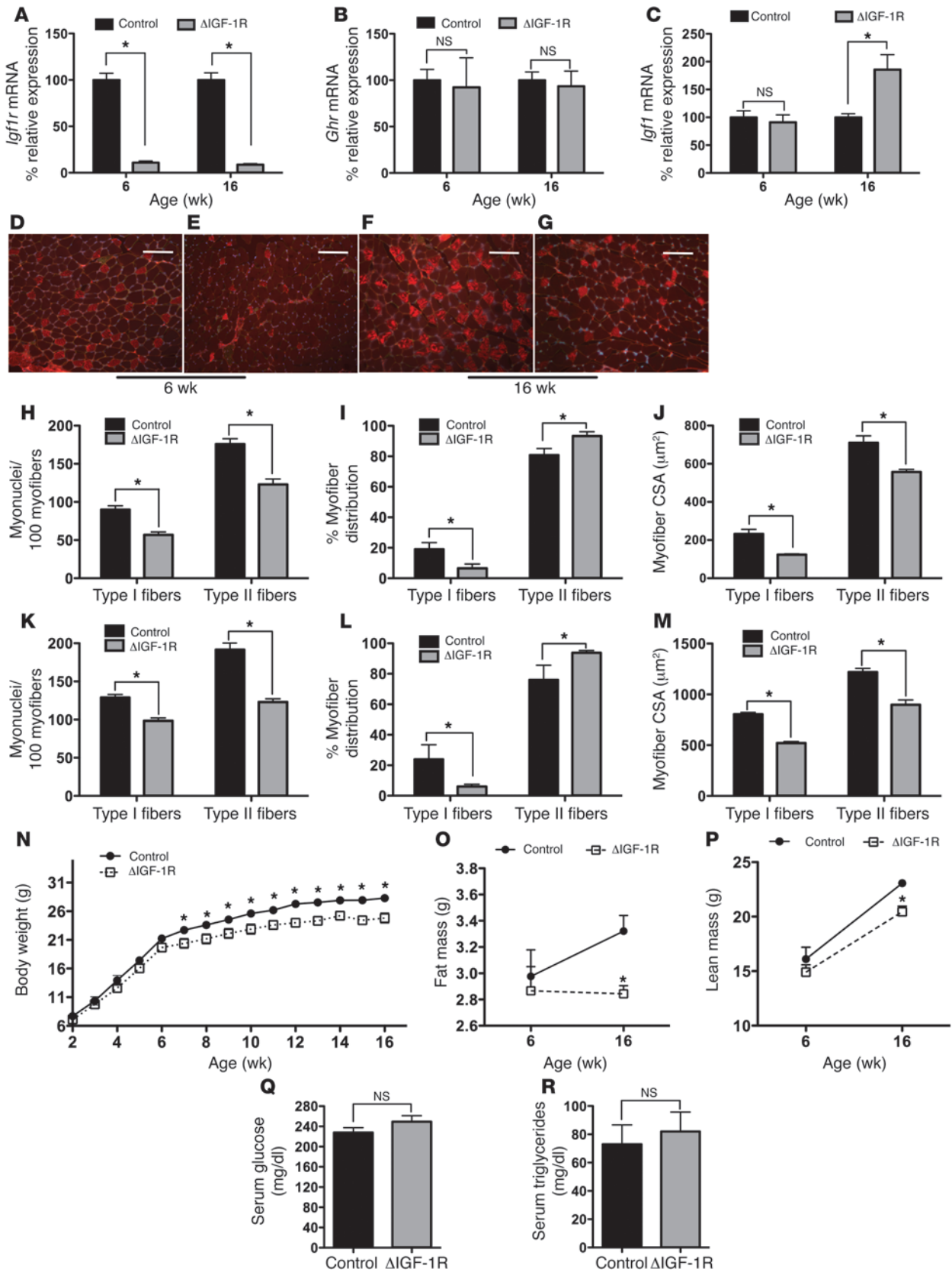
Figure 5

Mice lacking IGF-1R in skeletal muscle phenocopy the skeletal muscle defects of GHR mutants but are neither obese nor insulin resistant. mRNA was harvested from the gastrocnemius muscles of control and ΔIGF-1R mice, and real-time PCR was performed using primers for (**A**) *Igf1r*, (**B**) *Ghr*, and (**C**) *Igf1*. (**D**–**G**) Sections of gastrocnemius muscle from control and ΔIGF-1R mice were visualized using antibodies directed against MHC type I and laminin and counterstained with Hoechst 33258 to visualize myonuclei. Scale bars: 80 μm. (**H**–**M**) Histomorphometric analyses of myonuclei per 100 myofibers, percentage myofiber distribution, and myofiber diameter (CSA) were performed on sections described above for (**H**–**J**) 6-week-old and (**K**–**M**) 16-week-old control and ΔIGF-1R mice. (**N**) Control (*n* = 7) and ΔIGF-1R (*n* = 10) mice were weighed weekly from 2 to 16 weeks of age. qMR analysis of (**O**) fat and (**P**) lean mass in control and ΔIGF-1R mice at 6 and 16 weeks of age. Ad libitum (**Q**) serum glucose and (**R**) triglyceride levels were measured in control and ΔIGF-1R mice at 16 weeks of age. Unless otherwise indicated, *n* = 6 for control and ΔIGF-1R at all time points. Error bars indicate SEM. *$P < 0.05$.

decrease in total body lean mass (23.073 g in control vs. 20.438 g in ΔIGF-1R mice; *n* = 6; *P* < 0.002), with no change in total body bone mineral density (BMD) in ΔIGF-1R mice (0.050 g/cm² for control versus 0.048 g/cm² for ΔIGF-1R mice; *n* = 6; *P* = 0.131). Taken together, these results indicate a disturbance of muscle development in ΔIGF-1R mice, which is similar to that of ΔGHR mutants, but occurs in the absence of accompanying metabolic features or insulin resistance.

Discussion

GH is one of the most important factors that regulates postnatal longitudinal growth, body weight, and body composition in mammals (18, 41–45). GH exerts anabolic actions in skeletal muscle by both promoting muscle development and facilitating nutrient uptake and utilization in the muscle, thereby coordinating global energy expenditure and body composition (46, 47). However, the GH and IGF-1 pathways are so intimately connected that it has been challenging to distinguish actions of GH that result secondary to GH-induced IGF-1 production, as opposed to those that might be mediated by direct GHR signaling pathways. In this study, we used a genetic approach in mice to determine the requirement of different components of the GH/IGF-1 system in skeletal muscle development and postnatal function. Understanding the precise modes and mechanisms of GH action in skeletal muscle is essential for developing the most effective therapies to treat sarcopenia in aging humans, cachexia associated with cancer or AIDS, or a number of other muscle-wasting conditions.

Our studies demonstrate that the GHR is required for normal skeletal muscle development and provide several lines of evidence that the effects of GH on skeletal muscle development are mediated by muscle production of IGF-1. First, acute exposure of myoblasts to GH did not affect their proliferative rate, whereas IGF-1 treatment increased both myoblast proliferation and fusion, even in cells lacking GHR. The signals generated in myoblasts, after exposure to either GH or IGF-1, appear to activate the NFATc2/IL-4 pathway, previously shown to be critical for myoblast fusion (6). Therefore, while both GH and IGF-1 are capable of inducing NFAT translocation and activity (Figure 1, F and G), IGF-1 signaling appears to be predominate in controlling myoblast fusion and myonuclei accumulation. In accordance with this, treatment of ΔIGF-1R myoblasts with GH failed to increase myoblast fusion,

while treatment with exogenous IL-4 increased the fusion index (the percentage of fused myoblasts) but not the number of nuclei per myotube (Supplemental Figure 1, I and J). This result suggests that additional pathways, either in parallel to or downstream of NFATc2 and IL-4 activation, might also be activated by IGF-1 to induce myoblast fusion and accumulation of additional myonuclei. For example, IGF-1 is known to activate the PI-3K/Akt pathway to inhibit GSK3 and activate mTOR/p70S6K to induce myotube hypertrophy (48). Regardless of the downstream pathways activated, IGF-1 signaling appears to be vital for GH-induced myoblast fusion. Second, elimination of the IGF-1R from myoblasts abolished GH-induced myoblast fusion. Third, the skeletal muscle phenotypes resulting from disruption of GHR and IGF-1R were strikingly similar. These findings support previous observations in mice with unrestricted disruption of IGF-1R (49) or expression of a dominant-negative IGF-1R (35), which also exhibited hypoplastic skeletal muscle. Taken together, these data provide strong evidence that GH actions on skeletal muscle development require local IGF-1 production. It should be noted that this conclusion is the opposite of that reached by Sotiropoulos et al. (10), who reported that GH increased skeletal muscle cell fusion but suggested that this effect was directly mediated by GH, since GH did not induce IGF-1 in their cells. The exact reasons for these different results regarding the role of IGF-1 in skeletal muscle development are unclear but may relate to the different skeletal muscle cell models and/or differences in the timing of measurements of *Igf1* mRNA expression.

The histomorphometric changes observed in gastrocnemius muscles of the ΔGHR and ΔIGF-1R mice are compatible with our in vitro findings and strengthen the conclusion that GH promotes skeletal muscle development through myoblast-produced IGF-1. Skeletal muscle lacking either receptor had fewer myonuclei and smaller myofiber diameters. At 6 weeks of age, type I fiber distribution was lower in both mutants, although this defect persisted only in ΔIGF-1R mice at 16 weeks. These results suggest that GH normally functions to control type I fiber specification, likely through local IGF-1 production. Previous findings from mice globally deficient for the GHR exhibited significant reductions in soleus muscle type I fiber number and fiber diameter of soleus muscle (10). In addition, studies in humans have demonstrated a link between GH and fiber type specification. For example, in GH-deficient humans, the number of type I myofibers are significantly reduced in the vastus lateralis (50). These changes, together with the reduced myofiber diameters observed in the ΔGHR mice, most likely account for their reduced functional performance (grip strength and rotarod). In addition to these gross anatomical changes, it is probable that loss of GH/IGF-1 signals also compromises excitation-contraction coupling events. Consistent with this notion, preliminary assessment of showed that the force-generating capacity of single myofibers from ΔIGF-1R mice was reduced compared with that of controls (data not shown). Finally, we also created a model that lacked the IGF-1 ligand, specifically in skeletal muscle, using the same mef2c-Cre mouse used to generate the ΔGHR and ΔIGF-1R mice. Mice lacking IGF-1 had no discernible phenotype, and their body weights were indistinguishable from control littermates at all postnatal times (data not shown). We speculate that the normal muscle development of the ΔIGF-1 mice might be due to compensatory activity of local anabolic factors, including IGF-2 (51, 52). Together, these results indicate that loss of GHR and the atten-

dant reduction in myoblast IGF-1/IGF-1R signaling leads to deregulated fiber type specification, reduced muscle size, and subsequent compromised muscle function.

Surprisingly, loss of GHR in skeletal muscle was accompanied by a progressive increase in body weight and accumulation of peripheral fat. While nighttime voluntary locomotion was decreased in ΔGHR mice, food intake decreased and metabolic rate tended to increase in the mutants. We therefore assumed that the decreased nocturnal activity was likely not the causative factor for the observed increase in fat mass. Rather, we suspected that loss of GHR from skeletal muscle caused alterations of global nutrient metabolism. Indeed, serum glucose in the fed state was elevated in ΔGHR mutants, and the development of insulin resistance in these mice was confirmed by GTTs and ITTs. This finding might seem paradoxical, given that global GH resistance in mice that lack GHR/GH binding protein results in increased insulin sensitivity (53–59). However, GHR/GH binding protein mutant mice exhibit increased liver IR abundance and enhanced hepatic insulin-stimulated IR tyrosine phosphorylation (59–61), which likely accounts for their increased insulin sensitivity. Therefore, it would appear that the different metabolic profile exhibited by our ΔGHR mice, which lack GHR exclusively in skeletal muscle, is explained partially by maintenance of insulin action in nonskeletal muscle tissues in which GHR remains intact. It should also be noted that serum insulin remained unchanged in ΔGHR mice at all time points examined, further supporting normal insulin action and regulation in other insulin-responsive tissues. Taken together, the increased serum glucose and triglyceride levels observed in ΔGHR mice, in the face of normal insulin levels, suggests a failure of nutrient uptake by skeletal muscle. We predict that the increased fat mass observed in ΔGHR mutants results from redistribution of this nutrient supply from skeletal muscle to GHR-intact adipose tissue.

Importantly, the body composition and metabolic alterations seen in ΔGHR mice were not observed in ΔIGF-1R mice, which had reduced body weights, decreased peripheral fat, and normal, non-fasting serum glucose levels. These findings clearly suggest that the changes in body composition and insulin resistance seen in the ΔGHR mice are not due to loss of IGF-1 signaling in muscle. Rather, the actions of IGF-1 seem to be restricted primarily to anatomical development of the skeletal muscle. Interestingly, mice rendered IGF-1 resistant in skeletal muscle by targeting overexpression of a dominant-negative IGF-1R in skeletal muscle (MKR mice), exhibited metabolic disturbances similar to those observed in our ΔGHR mice, including increased peripheral fat and insulin resistance (62). In the MKR mice, expression of the dominant-negative IGF-1R effectively disrupts both IGF-1R and IR signaling by inducing formation of nonfunctioning hybrids between the mutant and the endogenous IGF-1 and IRs. By contrast, we propose that insulin signaling is attenuated in the ΔGHR mice due to decreased IR abundance and increased phosphorylation of IRS-1 on Ser 1101 (39), which together inhibit insulin signaling. Thus, the MKR mice and ΔGHR mice share a similar metabolic phenotype as a result of compromised IR signaling in skeletal muscle, which is manifested through distinct mechanisms. These defects in insulin signaling most likely represent the primary reason for the development of insulin resistance and increased peripheral adiposity in both models.

Our studies also shed light on the molecular mechanisms responsible for the development of insulin resistance in skeletal muscle from the ΔGHR mice. Since myoblasts lacking STAT5ab were also less sensitive to insulin-induced glucose uptake, it would appear that GH modulates insulin sensitivity, at least in part, through STAT5. Indeed, a number of genes modulating glucose and triglyceride uptake and metabolism are known to be regulated through GH-induced STAT5 activation (63). Accordingly, mice lacking STAT5ab in skeletal muscle also had increased fat mass, further suggesting the involvement of GH-induced STAT5-mediated genes in the metabolic effects seen in our ΔGHR mice (64, 65). However, the reduction of insulin-induced glucose uptake seen in ΔSTAT5ab myoblasts was not as pronounced as that of ΔGHR myoblasts, indicating the contribution additional pathways in the development of insulin resistance. As mentioned above, insulin resistance in myotubes lacking GHR appears to derive from changes at a number of proximal and distal points along the insulin signaling pathway, including decreased IR abundance, reduced basal Akt (Thr 308) and Erk phosphorylation, and the increased Ser 1101 phosphorylation of IRS-1 already discussed. Basal phosphorylation of other known inhibitory IRS-1 residues (Ser 612 and Ser 636/639) was reduced, at least in the context of our in vitro model system. However, it remains possible that the hyperglycemic, hypertriglyceridemic, and likely inflammatory conditions experienced in vivo may further exacerbate insulin resistance in skeletal muscle through pathways known to act on these inhibitory IRS-1 residues (66, 67). Since IR signals primarily through the PI-3K pathway, it is more likely that the reduction in basal Erk activation is a result of GHR disruption. However, loss of GH-mediated Erk activity could have indirect effects to further suppress insulin-induced glucose uptake in ΔGHR myoblasts. Erk interacts with TSC2 (68) to relieve its suppression of mTOR, allowing GLUT expression and glucose uptake (69), and the ability of GH to alter insulin sensitivity via nutrient-sensing pathways, like PI3K/mTOR/S6K (70), is currently being investigated.

In conclusion, the results presented in this paper indicate 2 circumscribed roles for GHR signaling is skeletal muscle. First, by regulating myoblast production of IGF-1, GH promotes normal myofiber type specification, myonuclei accumulation, and expansion of myofiber diameter, processes which are required for development of fully functional skeletal muscle. Second, GH functions independent of IGF-1R signaling to facilitate normal insulin action in skeletal muscle, which ultimately impacts global nutrient metabolism. Precisely how these distinct GH-generated signals are compartmentalized within skeletal muscle is a question currently under investigation in our laboratory. Further elucidation of these mechanisms should guide more informed use of GH or GH analogs for promoting muscle development and attenuating muscle loss as well as provide alternative means to affect insulin sensitivity and global nutrient metabolism across a range of metabolic syndromes.

Methods

Primary myoblast isolation and culture. Primary myoblast cultures were prepared from tibialis anterior and gastrocnemius muscles of 4-week-old wild-type, floxed GHR, and IGF-1R mice and purified to more than 99% as previously described (36). Growth media (GM) consisted of Ham's F-10, 20% FBS, 5 ng/ml basic recombinant human FGF (bFGF) (Promega), 100 U/ml penicillin G (GIBCO BRL), and 100 µg/ml streptomycin (GIBCO BRL). Myoblasts were grown in type I collagen-coated (BD Biosciences) plates. Fusion was induced by growing myoblasts in Entactin-Collagen-Laminin–coated (ECL-coated) (Upstate Biotechnology) dishes and low-serum differentiation media (DM) (DMEM with 1% insulin-transferrin-selenium-A

supplement [GIBCO BRL]). For in vitro deletion of the GHR, myoblasts with the floxed GHR alleles were cultured to be 80% confluent and then infected with an adenovirus encoding Cre recombinase (adenoCre) (Vector Biolabs) at a titer of 100 MOI in a small volume of sterile PBS. Myoblasts infected with 100 MOI of adenovirus encoding GFP (adenoGFP) (Vector Biolabs) were used as control. One hour after infection with adenovirus, GM were added to myoblasts and cultured for the next 48 hours. GHR deletion was confirmed for every infection by real-time PCR and immunoblotting with anti-GHR antibody (71). AdenoGFP-infected (referred to as control) or adenoCre-infected (referred to as ΔGHR) primary myoblasts were replated in 6-well plates for proliferation and fusion assays. ΔIGF-1R and ΔSTAT5 myoblasts were generated in an analogous manner.

Proliferation and fusion assays. Myoblasts were plated in 6-well type I collagen-coated plates at low cell density (1×10^5 cells/well of a 6-well plate) and cultured in Ham's F-10 media with 1% FBS for 10 hours to arrest the cells in G_0 phase. Cells were treated with 500 ng/ml GH, 100 ng/ml IGF-1, or 20% serum and 5 ng/ml bFGF and pulsed with 10 µM BrdU for the next 8 hours. Myoblasts were stained for anti-BrdU–APC and 7-amino-actinomycin D (APC BrdU Flow Kit, BD Biosciences) for proliferation and analyzed by FACSCalibur (Becton Dickinson). A total of 10,000 events were collected for each sample, and results were analyzed with WinMDI version 2.8. For fusion assays, after 24 or 48 hours in DM, myoblasts were fixed in 3.7% formaldehyde for 10 minutes. Cell membranes were identified by staining with 10 µM 1,1-dioctadecyl-3,3,3′,3′-tetramethylcarbocyanine perchlorate (DiI), while nuclei were identified by staining with 300 nM DAPI. The number of nuclei were counted and expressed as the number per DiI-labeled myotube.

Real-time PCR analysis. Total RNA was extracted from cells using the TRIzol method, as recommended by the manufacturer (catalog 15596-026, Invitrogen). RNA concentration was estimated spectrophotometrically, and only pure RNA (A_{260}/A_{280} ratio of 1.8) was used for further analysis. First-strand cDNA was synthesized using the iScript cDNA Synthesis Kit (Bio-Rad Laboratories). The cDNA was amplified in the Opticon Continuous Fluorescent Detector (MJ Research) using iQ SYBR Green Supermix (Bio-Rad) and sequence specific primers according to the manufacturer's instructions. A total of 1 µg RNA was used in each reaction and combined with specific primers. Primer sequences used were as follows: *Ghr*, forward 5′-AGCCTCGATTCACAAGTGTCG-3′, reverse 5′-GATGACCAATTCTTG-CAGCTTG-3′; *Igf1r*, forward 5′-TTGTGTTGTTCGTCCGGTGTG-3′, reverse 5′-ATGTGCCCAAGTGTGTGCG-3′; *Igf1*, forward 5′-GCTCTTCAGTTC-GTGTGTGGAC-3′, reverse 5′-TTGGGCTGTCAGTGTGGCGC-3′; *Actb*, forward 5′-ACCTCCTACAATGAGCTGC-3′, reverse 5′-TGCCAATAGTGAT-GACCT-3′; *Pax7*, forward 5′-CACCCCGGGGACAGAGGAAGAT-3′, reverse 5′-GAGAGGGCGGGGTACAAGGAAGAC-3′; *Myf5*, forward 5′-AGCCCAC-CAGCCCCACCTC-3′, reverse 5′-TTCTGCCCAGCTTGTCTTTCCTTC-3′; *Cdh15*, forward 5′-CATCCCACCCATTAGTGTGTC-3′, reverse 5′-TCCCAGTGAACTTGTCGATAGA-3′; *Des*, forward 5′-GTGGATGCAGC-CACTCTAGC-3′, reverse 5′-TTAGCCGCGATGGTCTCATAC-3′; *Myod1*, forward 5′-ACACTTCTGGCCCGAGGTAT-3′, reverse 5′-GACTTCCAAT-GTTTCATCAGTGC-3′; *Myog*, forward 5′-GAGACATCCCCCTATTTC-TACCA-3′, reverse 5′-GCTCAGTCCGCTCATAGCC-3′; *Myh3*, forward 5′-CCTTGGCACCAATGTCCCGGCTC-3′, reverse 5′-GAAGCGCAATG-CAGAGTCGGTG-3′; *Il4*, forward 5′-AACCCCCAGCTAGTTGTCATCCTG-3′, reverse 5′-CATCGAAAAGCCCGAAAGAGTCTC-3′. PCR was performed in triplicate for each cDNA, and results were averaged and normalized to endogenous β-actin reference transcripts.

Cell lysis and immunoblot analysis. To collect cell lysates for immunoblot analysis, myoblasts were washed twice with ice-cold PBS and resuspended in cell lysis buffer (50 mM Tris, pH 7.4, 150 mM NaCl, 1 mM MgCl₂, 1 mM EDTA, 1% Triton X-100, and 10% glycerol) containing protease and phosphatase inhibitors (Sigma-Aldrich). Cell lysates were homogenized by rotating at 4°C

for 30 minutes and then centrifuged at 8,700 *g* for 20 minutes at 4°C. Supernatant was transferred to microcentrifuge tubes, and protein concentration was measured using Bradford protein assay (Bio-Rad). For immunoblotting of whole cell lysates, equal amounts of protein (10 µg/lane) were solubilized in Laemmli sample buffer and loaded onto a mini–SDS-PAGE system. Following electrophoresis, proteins were transferred to a polyvinylidene difluoride membrane using a Bio-Rad wet transfer system. Protein transfer efficiency was verified using prestained protein markers. Membranes were blocked with 5% nonfat dry milk for 1 hour at room temperature and subsequently incubated overnight at 4°C with antibodies directed against the protein of interest. Signals were detected using a horseradish peroxidase–conjugated secondary antibody, and bound antibodies were visualized using the Supersignal West Dura Substrate (Pierce). Western blot photographic results were scanned with a Canon flatbed scanner. Proteins in the cytoplasm and nuclear fractions were separated using NE-PER nuclear and cytoplasmic extraction reagents according to the manufacturer's instructions (Pierce Biotechnology Inc.). Antibodies used were as follows: anti–IGF-1R β-subunit (C-20), anti–β-actin (C4), and anti–α-tubulin all from Santa Cruz Biotechnology Inc.; anti-GHR (AL47) antibody (71); and anti–phospho-Erk1/2, anti-Erk1/2, anti-IR, anti–phospho-IRS-1 (Ser 1101, Ser 612, and Ser 636/639), anti–IRS-1, anti–phospho-Akt (Thr 308 and Ser 473), and anti-Akt all from Cell Signaling Technology. Horseradish peroxidase–conjugated rabbit and mouse secondary antibodies were obtained from Pierce Biotechnology Inc. Polyvinylidene difluoride membrane, Laemmli sample buffer, and other electrophoresis supplies were obtained from Bio-Rad. Densitometry was performed using the analysis feature of Adobe Photoshop CS4. Briefly, images were converted from 8-bit RGB to grayscale, and a single, uniform selection box was used to collect mean gray density values for each band of interest. These values were normalized to similar measurements performed for relevant loading control proteins. Quantitation from multiple experiments ($n \geq 3$) was graphed, and the results are presented with representative blots.

NFAT luciferase reporter assay. For transient transfections, primary myoblasts were grown in 6-well plates at 2.5×10^5 cells per well. For each well, 2 µg NFAT reporter construct DNA (a gift from Majd Zayzafoon, University of Alabama at Birmingham) was complexed with 2 µl FuGENE HD Transfection Reagent (Roche) for 10 minutes at room temperature in a total volume of 500 µl of Ham's F10 media. The DNA-FuGENE mixture was added to the wells containing 2 ml of Ham's F10 media and incubated overnight at 37°C. Twenty-four hours after transient transfection with the NFAT reporter construct, myoblasts were plated at 7.5×10^5 cells per well of the ECL-coated 24-well plate. Myoblasts were allowed to settle, and the medium was replaced with DM to induce fusion for a duration of 24 hours. Following this, cells were treated with 500 ng/ml bovine GH or 100 ng/ml IGF-1 or 1 µM ionomycin for 5 hours and assayed for luciferase expression.

Measurement of 2-doG uptake. Myoblasts were plated in 12-well plates (1×10^5 cells/well) and cultured in Ham's F-10 with 20% FBS for 5 hours. Myoblasts were serum starved in 0.1% Ham's F-10 media for 12 hours and washed with Krebs-Ringer phosphate HEPES buffer (KRPH buffer, 136 mM NaCl, 4.7 mM KCl, 1.25 mM MgSO₄, 1.25 mM CaCl₂, and 20 mM HEPES, pH 7.4) in 0.2% BSA. Cells were then incubated with or without 10 nM insulin in 900 µl of KRPH buffer in 0.2% BSA for 1 hour at 37°C. For [³H]2-doG uptake, 50 µl reaction mixture, containing 5 µCi 2-[1,2-³H]-deoxy-D-glucose (PerkinElmer) and 1 mM 2-doG, was added to each well for 3 minutes at room temperature. The reaction was stopped by washing cells 3 times in ice-cold KRPH buffer containing 0.3 mM phloretin. Next, cells were lysed using 500 µl 1 N NaOH at 50°C for 30 minutes, followed by addition of 500 µl 1 N HCl to neutralize NaOH. The incorporated radioactivity was determined by liquid scintillation counting, and specific uptake (i.e., the background subtracted from the total uptake) was obtained. Assays were performed in triplicate, and data are presented as picomoles of 2-doG per milligram protein per minute.

Generation of skeletal muscle–specific GHR and IGF-1R ligand knockout mice. To generate the knockout mice, GHR (72) or IGF-1R (31, 73) homozygous floxed mice (*Ghr^fl/fl* or *Igf1r^fl/fl* mice) were crossed with mice that express the Cre recombinase specifically in skeletal muscle, under the control of the mef-2c-73k promoter (heterozygous mef-2c-73kCre^+/– mice) (a gift from Brian Black, University of California San Francisco, San Francisco, California, USA).The F1 transheterozygote progeny from this mating (i.e., *Ghr^fl/+*/mef-2c-73kCre^+/– mice) were then crossed with the homozygous floxed animals (i.e., *Ghr^fl/fl* mice) to produce the Cre-positive knockout animals (ΔGHR or ΔIGF-1R mice) and Cre-negative littermate controls (i.e., *Ghr^fl/fl*/mef-2c-73kCre^+/– and *Ghr^fl/fl*/mef-2c-73kCre^-/– mice, respectively). All animals were on a mixed genetic background of 129SVJ and C57BL/6. Mice were fed ad libitum and weighed weekly. All studies were performed in male mice. The Institutional Animal Care and Use Committee of the University of Alabama at Birmingham approved all animal work.

Histomorphometric analysis. Gastrocnemius muscles were embedded in OCT-embedding media, and mounts were cut in 5-μm serial sections at –22°C using a Leica CM1900 cryostat microtome. Slides were kept in a humidified chamber throughout the staining protocol. Sections were fixed for 45 minutes at room temperature in 3% neutral-buffered formalin and washed twice for 5 minutes with 1x PBS (all subsequent PBS wash steps were 3 × 5 minutes). Sections were blocked with 5% goat serum in PBS for 20 minutes at room temperature, followed by a wash step. Primary and secondary antibodies were diluted in 1% goat serum in PBS. Anti-MHC type I (anti–MHC I) primary antibody (mouse mAb NCL-MHCs, NovoCastra Laboratories; 1:100) was applied for 30 minutes at 37°C. After a wash step, sections were incubated with Alexa Fluor 594–conjugated goat anti-mouse secondary antibody (Pierce Biotechnology Inc.; 1:200) for 30 minutes at 37°C. Sections were washed and again blocked (5% goat serum in PBS) for 20 minutes at room temperature. To locate sarcolemma for myofiber sizing, a wash step was followed by incubation with anti-laminin mouse mAb (VP-L551, NovoCastra Laboratories; 1:80) for 30 minutes at 37°C, a wash step, and incubation with Alexa Fluor 488–conjugated goat anti-mouse secondary antibody (Pierce Biotechnology Inc.; 1:200) for 30 minutes at 37°C. Nuclei were revealed using a Hoecsht 33258 DNA counterstain (Molecular Probes; 1:10,000 in PBS) for 2 minutes at room temperature. Slides underwent a final aspiration and were mounted with 1% paraphenylene diamine and 90% glycerol in PBS. Slides and coverslips were bound together using nail polish and stored, protected from light, at –20°C.

Immunofluorescence microscopy. High-resolution (48-bit TIFF) images were captured at magnifications of ×10 and ×20, using an Olympus MagnaFire SP camera (S99810) and MagnaFire SP (http://download.optronics.com/02-camera-download-details.asp?ProductTable_ID=23) with an Olympus BX51 fluorescent microscope. Image analysis was performed using Image-Pro Plus 5.0 software. All analyses were conducted by a single analyst, who was blinded to the age and the genotype of each sample. Myofiber-type distribution was determined from 935 ± 47 myofibers per sample. Myofibers negative for MHC I were classified as type II fibers. For cross-sectional area (CSA) measurements, each myofiber was manually traced along its laminin-stained border. CSA (in μm²) was calibrated using a stage micrometer, and only those fibers determined to be cross-sectional based on a roundness factor of less than 1.639 were included in the analysis (roundness = perimeter^2/4$_\pi$ area; perfect circle = 1.0, pentagon = 1.163, square = 1.266, equilateral triangle = 1.639).

Assessment of body composition. All body composition scans were performed in the morning. Mice were anesthetized with isoflurane (2%), and body composition was assessed in vivo using DXA (GE Lunar PIXImus software version 1.45, Lunar) at 6, 16, and 26 weeks. Fat mass and soft lean tissue mass were determined as described previously (74). Briefly, mice were anesthetized and placed in a prostrate position on the imaging plate, and a total body scan was done in approximately 5 minutes. All analyses were done excluding the head. qMR was performed without sedation in less than 90 seconds for the noninvasive determination of fat and lean mass (3-in-1 Composition Analyzer, Echo Medical Systems).

Analysis of skeletal muscle function. For the grip strength test, mice were held by the base of the tail above a wire grid and gently lowered down until all 4 paws grasped the grid. Mice were then maneuvered to a horizontal position and gently pulled by the tail until they released the grip. Maximal force achieved by the animal was recorded for 3 successive trials and averaged. For the rotarod test, the rotating drum was set to accelerate from 4 to 40 rpm over 300 seconds; 30 minutes were left between training and test sessions and 15 minutes were left between each test session. Speed of rotation was constant upon reaching 40 rpm. Three trials were performed, and duration on the rotating rod and rotating distance measured were averaged.

Necropsy and tissue processing. Mice were sacrificed at 6, 16, or 26 weeks and whole body necropsy was performed. Fat pads (inguinal, gonadal, retroperitoneal, subcutaneous, mesenteric, and brown adipose tissue), livers, and hearts were removed and weighed. Gastrocnemius, soleus, and tibialis anterior muscles were dissected, weighed and snap frozen in liquid nitrogen, and stored at –80°C. Blood was allowed to clot at room temperature, and serum was separated by centrifugation and stored at –80°C until further analysis.

Serum analysis. Triglyceride, insulin, and glucose levels were measured in 10 μl samples of serum with the Ektachem DT II System (Johnson & Johnson Clinical Diagnostics). Total nonesterified FFAs were measured using an enzymatic, colorimetric method ("NEFA-C" reagents, Wako Diagnostics) modified to a microplate format.

Energy expenditure, locomotor activity tests, and food intake. Total energy expenditure (TEE) and locomotor activity for individually housed mice were analyzed using an indirect-calorimetric system (Labmaster, TSE Systems GmbH). Mice were placed in air-tight respiratory chambers with a flow rate of 0.45 l/h and placed at a constant temperature (22.0°C ± 1.0°C). Energy expenditure was calculated using 2-minute sample O_2 and CO_2 concentrations for quantification of O_2 consumption and CO_2 production. TEE was determined by calculating the average hourly energy expenditure over 22 hours and then multiplied by 24. Resting energy expenditure (REE) was calculated by averaging the 3 lowest 10-consecutive-minute periods of energy expenditure, with at least 1 hour between each period. This was then multiplied to generate a 24-hour REE. Detection of locomotor activity within the chambers was performed with an infrared sensor arranged in a grid pattern for horizontal (x, y level) activity. Movement was monitored continuously and recorded by the computer every 9 minutes. Locomotor activity was calculated by total counts every 9 minutes and expressed as counts per 24 hours. All above experiments were performed under red light to avoid changes in circadian rhythmic activity. Food consumption was determined by measuring the loss of food from the hopper of each animal over a 3-day period.

Assessment of glucose disposal and insulin sensitivity. For ITTs, mice were fasted for 4 hours and injected with insulin (0.2 U/kg body weight) i.p. Blood was collected from the tail vein and monitored for glucose, using blood glucose strips and a glucometer every 15 minutes for 2 hours. ITT data were calculated as percentage of initial blood glucose concentration. For GTTs, mice were injected with glucose (1.5 g/kg body weight) i.p. after an overnight fast (~16 hours), and blood glucose levels were measured every 15 minutes for 2 hours.

Statistics. All statistical analysis was performed using the Student's *t* test (2-tailed). Error bars represent SEM. P values of less than 0.05 are considered to be statistically significant.

Acknowledgments

Address correspondence to: Thomas L. Clemens, 601 N. Caroline St., JHOC 5242, Baltimore, Maryland 21287-0882, USA. Phone: 410.955.3245; Fax: 410.614.1451; E-mail: tclemen5@jhmi.edu.

Mahendra D. Mavalli's present address is: Department of Pathology, University of Alabama at Birmingham, Birmingham, Alabama, USA.

1. Kablar B, et al. MyoD and Myf-5 define the specification of musculature of distinct embryonic origin. *Biochem Cell Biol*. 1998;76(6):1079–1091.
2. Hasty P, et al. Muscle deficiency and neonatal death in mice with a targeted mutation in the myogenin gene. *Nature*. 1993;364(6437):501–506.
3. Nabeshima Y, Hanaoka K, Hayasaka M, Esumi E, Li S, Nonaka I. Myogenin gene disruption results in perinatal lethality because of severe muscle defect. *Nature*. 1993;364(6437):532–535.
4. Horsley V, Pavlath GK. Forming a multinucleated cell: molecules that regulate myoblast fusion. *Cells Tissues Organs*. 2004;176(1–3):67–78.
5. Horsley V, Friday BB, Matteson S, Kegley KM, Gephart J, Pavlath GK. Regulation of the growth of multinucleated muscle cells by an NFATC2-dependent pathway. *J Cell Biol*. 2001;153(2):329–338.
6. Horsley V, Jansen KM, Mills ST, Pavlath GK. IL-4 acts as a myoblast recruitment factor during mammalian muscle growth. *Cell*. 2003;113(4):483–494.
7. Baum HB, et al. Effects of physiologic growth hormone therapy on bone density and body composition in patients with adult-onset growth hormone deficiency. A randomized, placebo-controlled trial. *Ann Intern Med*. 1996;125(11):883–890.
8. Ullman M, Oldfors A. Effects of growth hormone on skeletal muscle. I. Studies on normal adult rats. *Acta Physiol Scand*. 1989;135(4):531–536.
9. Weber MM. Effects of growth hormone on skeletal muscle. *Horm Res*. 2002;58 suppl 3:43–48.
10. Sotiropoulos A, et al. Growth hormone promotes skeletal muscle cell fusion independent of insulin-like growth factor 1 up-regulation. *Proc Natl Acad Sci U S A*. 2006;103(19):7315–7320.
11. Kaplan S, Kostyo JL. Hormonal regulation of growth and metabolic effects of growth hormone. In: Kostyo JL, ed. *Handbook of Physiology*. Vol. 5. New York, New York, USA: Oxford University Press; 1999:129–143.
12. Zhang Y, Jiang J, Kopchick JJ, Frank SJ. Disulfide linkage of growth hormone (GH) receptors (GHR) reflects GH-induced GHR dimerization. Association of JAK2 with the GHR is enhanced by receptor dimerization. *J Biol Chem*. 1999;274(46):33072–33084.
13. Argetsinger LS, et al. Identification of JAK2 as a growth hormone receptor-associated tyrosine kinase. *Cell*. 1993;74(2):237–244.
14. Miller WL, Eberhardt NL. Structure and evolution of the growth hormone gene family. *Endocr Rev*. 1983;4(2):97–130.
15. Carter-Su C, Schwartz J, Smit LS. Molecular mechanism of growth hormone action. *Annu Rev Physiol*. 1996;58:187–207.
16. Davey HW, Xie T, McLachlan MJ, Wilkins RJ, Waxman DJ, Grattan DR. STAT5b is required for GH-induced liver IGF-I gene expression. *Endocrinology*. 2001;142(9):3836–3841.
17. Woelfle J, Billiard J, Rotwein P. Acute control of insulin-like growth factor-I gene transcription by growth hormone through Stat5b. *J Biol Chem*. 2003;278(25):22696–22702.
18. Lupu F, Terwilliger JD, Lee K, Segre GV, Efstratiadis A. Roles of growth hormone and insulin-like growth factor 1 in mouse postnatal growth. *Dev Biol*. 2001;229(1):141–162.
19. Liu JL, Yakar S, LeRoith D. Conditional knock-out of mouse insulin-like growth factor-1 gene using the Cre/loxP system. *Proc Soc Exp Biol Med*. 2000;223(4):344–351.
20. Yakar S, Liu JL, Le Roith D. The growth hormone/insulin-like growth factor-I system: implications for organ growth and development. *Pediatr Nephrol*. 2000;14(7):544–549.
21. Le RD, Bondy C, Yakar S, Liu JL, Butler A. The somatomedin hypothesis: 2001. *Endocr Rev*. 2001;22(1):53–74.
22. Yakar S, Wu Y, Setser J, Rosen CJ. The role of circulating IGF-I: lessons from human and animal models. *Endocrine*. 2002;19(3):239–248.
23. DiGirolamo DJ, et al. Mode of growth hormone action in osteoblasts. *J Biol Chem*. 2007; 282(43):31666–31674.
24. Adams GR, Haddad F. The relationships among IGF-1, DNA content, and protein accumulation during skeletal muscle hypertrophy. *J Appl Physiol*. 1996;81(6):2509–2516.
25. Goldspink G. Changes in muscle mass and phenotype and the expression of autocrine and systemic growth factors by muscle in response to stretch and overload. *J Anat*. 2010;194(pt 3):323–334.
26. Musaro A, et al. Localized Igf-1 transgene expression sustains hypertrophy and regeneration in senescent skeletal muscle. *Nat Genet*. 2001;27(2):195–200.
27. Owino V, Yang SY, Goldspink G. Age-related loss of skeletal muscle function and the inability to express the autocrine form of insulin-like growth factor-1 (MGF) in response to mechanical overload. *FEBS Lett*. 2001;505(2):259–263.
28. Favelyukis S, Till JH, Hubbard SR, Miller WT. Structure and autoregulation of the insulin-like growth factor 1 receptor kinase. *Nat Struct Biol*. 2001;8(12):1058–1063.
29. Ullrich A, et al. Insulin-like growth factor I receptor primary structure: comparison with insulin receptor suggests structural determinants that define functional specificity. *EMBO J*. 1986;5(10):2503–2512.
30. LeRoith D. Insulin-like growth factor I receptor signaling--overlapping or redundant pathways? *Endocrinology*. 2000;141(4):1287–1288.
31. Dietrich P, Dragatsis I, Xuan S, Zeitlin S, Efstratiadis A. Conditional mutagenesis in mice with heat shock promoter-driven cre transgenes. *Mamm Genome*. 2000;11(3):196–205.
32. Mohan S. Insulin-like growth factor binding proteins in bone cell regulation. *Growth Regul*. 1993;3(1):67–70.
33. Rajpathak SN, et al. The role of insulin-like growth factor-I and its binding proteins in glucose homeostasis and type 2 diabetes. *Diabetes Metab Res Rev*. 2009;25(1):3–12.
34. Laviola L, Natalicchio A, Giorgino F. The IGF-I signaling pathway. *Curr Pharm Des*. 2007;13(7):663–669.
35. Kim H, Barton E, Muja N, Yakar S, Pennisi P, LeRoith D. Intact insulin and insulin-like growth factor-I receptor signaling is required for growth hormone effects on skeletal muscle growth and function in vivo. *Endocrinology*. 2005;146(4):1772–1779.
36. Rando TA, Blau HM. Primary mouse myoblast purification, characterization, and transplantation for cell-mediated gene therapy. *J Cell Biol*. 1994;125(6):1275–1287.
37. Urban RJ, et al. Testosterone administration to elderly men increases skeletal muscle strength and protein synthesis. *Am J Physiol*. 1995;269(5 pt 1):E820–E826.
38. Gentile MA, et al. Androgen-mediated improvement of body composition and muscle function involves a novel early transcriptional program
including IGF1, mechano growth factor, and induction of {beta}-catenin. *J Mol Endocrinol*. 2010; 44(1):55–73.
39. Tremblay F, et al. Identification of IRS-1 Ser-1101 as a target of S6K1 in nutrient- and obesity-induced insulin resistance. *Proc Natl Acad Sci U S A*. 2007; 104(35):14056–14061.
40. Himpe E, Kooijman R. Insulin-like growth factor-I receptor signal transduction and the Janus Kinase/Signal Transducer and Activator of Transcription (JAK-STAT) pathway. *Biofactors*. 2009;35(1):76–81.
41. Cuneo RC, Salomon F, Wiles CM, Sonksen PH. Skeletal muscle performance in adults with growth hormone deficiency. *Horm Res*. 1990;33 suppl 4:55–60.
42. Cuneo RC, Salomon F, Wiles CM, Hesp R, Sonksen PH. Growth hormone treatment in growth hormone-deficient adults. I. Effects on muscle mass and strength. *J Appl Physiol*. 1991;70(2):688–694.
43. Mauras N, Attie KM, Reiter EO, Saenger P, Baptista J. High dose recombinant human growth hormone (GH) treatment of GH-deficient patients in puberty increases near-final height: a randomized, multicenter trial. Genentech, Inc., Cooperative Study Group. *J Clin Endocrinol Metab*. 2000; 85(10):3653–3660.
44. Mauras N, et al. Insulin-like growth factor I and growth hormone (GH) treatment in GH-deficient humans: differential effects on protein, glucose, lipid, and calcium metabolism. *J Clin Endocrinol Metab*. 2000;85(4):1686–1694.
45. Mauras N. Growth hormone therapy in the glucocorticosteroid-dependent child: metabolic and linear growth effects. *Horm Res*. 2001;56 suppl 1:13–18.
46. Cotes PM, Reid E, Young FG. Diabetogenic action of pure anterior pituitary growth hormone. *Nature*. 1949;164(4162):209–211.
47. Houssay BA, Rodriguez RR. Diabetogenic action of different preparations of growth hormone. *Endocrinology*. 1953;53(1):114–116.
48. Rommel C, et al. Mediation of IGF-1-induced skeletal myotube hypertrophy by PI(3)K/Akt/mTOR and PI(3)K/Akt/GSK3 pathways. *Nat Cell Biol*. 2001;3(11):1009–1013.
49. Liu JP, Baker J, Perkins AS, Robertson EJ, Efstratiadis A. Mice carrying null mutations of the genes encoding insulin-like growth factor I (Igf-1) and type 1 IGF receptor (Igf1r). *Cell*. 1993;75(1):59–72.
50. Daugaard JR, et al. Effect of 6 months of GH treatment on myosin heavy chain composition in GH-deficient patients. *Eur J Endocrinol*. 1999; 141(4):342–349.
51. Lovett FA, et al. Convergence of Igf2 expression and adhesion signalling via RhoA and p38 MAPK enhances myogenic differentiation. *J Cell Sci*. 2006; 119(pt 23):4828–4840.
52. Ren H, Yin P, Duan C. IGFBP-5 regulates muscle cell differentiation by binding to IGF-II and switching on the IGF-II auto-regulation loop. *J Cell Biol*. 2008; 182(5):979–991.
53. Bratusch-Marrain PR, Smith D, DeFronzo RA. The effect of growth hormone on glucose metabolism and insulin secretion in man. *J Clin Endocrinol Metab*. 1982;55(5):973–982.
54. Davidson MB, Shen DC, Venkatesan N, Sladen G. In vivo insulin antagonism but evanescent in vitro tissue effect in rats with growth hormone-secreting tumors. *J Endocrinol Invest*. 1987;10(6):569–574.
55. Rizza RA, Mandarino LJ, Gerich JE. Effects of growth

hormone on insulin action in man. Mechanisms of insulin resistance, impaired suppression of glucose production, and impaired stimulation of glucose utilization. *Diabetes*. 1982;31(8 pt 1):663–669.

56. Hopwood NJ, Forsman PJ, Kenny FM, Drash AL. Hypoglycemia in hypopituitary children. *Am J Dis Child*. 1975;129(8):918–926.

57. Bougneres PF, Artavia-Loria E, Ferre P, Chaussain JL, Job JC. Effects of hypopituitarism and growth hormone replacement therapy on the production and utilization of glucose in childhood. *J Clin Endocrinol Metab*. 1985;61(6):1152–1157.

58. Daugaard JR, Laustsen JL, Hansen BS, Richter EA. Insulin action in growth hormone-deficient and age-matched control rats: effect of growth hormone treatment. *J Endocrinol*. 1999;160(1):127–135.

59. Bonkowski MS, Rocha JS, Masternak MM, Al Regaiey KA, Bartke A. Targeted disruption of growth hormone receptor interferes with the beneficial actions of calorie restriction. *Proc Natl Acad Sci U S A*. 2006;103(20):7901–7905.

60. Coschigano KT, Holland AN, Riders ME, List EO, Flyvbjerg A, Kopchick JJ. Deletion, but not antagonism, of the mouse growth hormone receptor results in severely decreased body weights, insulin, and insulin-like growth factor I levels and increased life span. *Endocrinology*. 2003;144(9):3799–3810.

61. Panici JA, et al. Is altered expression of hepatic insulin-related genes in growth hormone receptor

knockout mice due to GH resistance or a difference in biological life spans? *J Gerontol A Biol Sci Med Sci*. 2009;64(11):1126–1133.

62. Kim CH, et al. MKR mice are resistant to the metabolic actions of both insulin and adiponectin: discordance between insulin resistance and adiponectin responsiveness. *Am J Physiol Endocrinol Metab*. 2006;291(2):E298–E305.

63. Hosui A, Hennighausen L. Genomic dissection of the cytokine-controlled STAT5 signaling network in liver. *Physiol Genomics*. 2008;34(2):135–143.

64. Klover P, Hennighausen L. Postnatal body growth is dependent on the transcription factors signal transducers and activators of transcription 5a/b in muscle: a role for autocrine/paracrine insulin-like growth factor I. *Endocrinology*. 2007;148(4):1489–1497.

65. Klover P, Chen W, Zhu BM, Hennighausen L. Skeletal muscle growth and fiber composition in mice are regulated through the transcription factors STAT5a/b: linking growth hormone to the androgen receptor. *FASEB J*. 2009;23(9):3140–3148.

66. Ozes ON, et al. A phosphatidylinositol 3-kinase/Akt/mTOR pathway mediates and PTEN antagonizes tumor necrosis factor inhibition of insulin signaling through insulin receptor substrate-1. *Proc Natl Acad Sci U S A*. 2001;98(8):4640–4645.

67. De Fea K, Roth RA. Protein kinase C modulation of insulin receptor substrate-1 tyrosine phosphorylation requires serine 612. *Biochemistry*. 1997;

36(42):12939–12947.

68. Ma L, Chen Z, Erdjument-Bromage H, Tempst P, Pandolfi PP. Phosphorylation and functional inactivation of TSC2 by Erk implications for tuberous sclerosis and cancer pathogenesis. *Cell*. 2005;121(2):179–193.

69. Buller CL, et al. A GSK-3/TSC2/mTOR pathway regulates glucose uptake and GLUT1 glucose transporter expression. *Am J Physiol Cell Physiol*. 2008;295(3):C836–843.

70. Hayashi AA, Proud CG. The rapid activation of protein synthesis by growth hormone requires signaling through mTOR. *Am J Physiol Endocrinol Metab*. 2007;292(6):E1647–1655.

71. Zhang Y, et al. Growth hormone (GH)-induced dimerization inhibits phorbol ester-stimulated GH receptor proteolysis. *J Biol Chem*. 2001;276(27):24565–24573.

72. Fan Y, et al. Liver-specific deletion of the growth hormone receptor reveals essential role of growth hormone signaling in hepatic lipid metabolism. *J Biol Chem*. 2009;284(30):19937–19944.

73. Fulzele K, DiGirolamo DJ, Liu Z, Xu J, Messina JL, Clemens TL. Disruption of the insulin-like growth factor type 1 receptor in osteoblasts enhances insulin signaling and action. *J Biol Chem*. 2007;282(35):25649–25658.

74. Nagy A. Cre recombinase: the universal reagent for genome tailoring. *Genesis*. 2000;26(2):99–109.